Glutamatergic neuronal activity regulates angiogenesis and blood-retinal barrier maturation via Norrin/β-catenin signaling

Saptarshi Biswas[1,*], Sanjid Shahriar[2, 3], Galina Bachay[4], Panos Arvanitis[5], Danny Jamoul[1, 6], William J. Brunken[4] and Dritan Agalliu[1, 2, *]

[1]Department of Neurology, Columbia University Irving Medical Center, New York, NY 10032, USA.

[2]Department of Pathology and Cell Biology, Columbia University Irving Medical Center, New York, NY 10032, USA.

[3]Wyss Institute for Biologically Inspired Engineering, Boston, MA 02115, USA.

[4]Department of Ophthalmology and Visual Sciences, SUNY Upstate Medical University, Syracuse, NY 13210, USA.

[5]Warren Alpert Medical School, Brown University, Providence, RI 02903, USA.

[6]John Jay College of Criminal Justice, City University of New York, New York, NY 10019, USA.

***Corresponding authors:**

Saptarshi Biswas Ph.D. Email – sb4082@cumc.columbia.edu

Dritan Agalliu Ph.D. Email – da191@cumc.columbia.edu

Lead contact:

Dritan Agalliu Ph.D. Email – da191@cumc.columbia.edu

Keywords:

Glutamate, neuronal activity, angiogenesis, blood-retinal barrier, tight junctions, Norrin/β-catenin signaling

SUMMARY

Interactions among neuronal, glial and vascular components are crucial for retinal angiogenesis and blood-retinal barrier (BRB) maturation. Although synaptic dysfunction precedes vascular abnormalities in many retinal pathologies, how neuronal activity, specifically glutamatergic activity, regulates retinal angiogenesis and BRB maturation remains unclear. Using *in vivo* genetic studies in mice, single-cell RNA-sequencing and functional validation, we show that deep plexus angiogenesis and paracellular BRB maturation are delayed in *Vglut1*$^{-/-}$ retinas where neurons fail to release glutamate. In contrast, deep plexus angiogenesis and paracellular BRB maturation are accelerated in *Gnat1*$^{-/-}$ retinas where constitutively depolarized rods release excessive glutamate. Norrin expression and endothelial Norrin/β-catenin signaling are downregulated in *Vglut1*$^{-/-}$ retinas, and upregulated in *Gnat1*$^{-/-}$ retinas. Pharmacological activation of endothelial Norrin/β-catenin signaling in *Vglut1*$^{-/-}$ retinas rescued defects in deep plexus angiogenesis and paracellular BRB maturation. Our findings demonstrate that glutamatergic neuronal activity regulates retinal angiogenesis and BRB maturation by modulating endothelial Norrin/β-catenin signaling.

38 **INTRODUCTION**

39 The crosstalk among neuronal, glial, and vascular components is essential, not only for proper angiogenesis,
40 but also for the establishment of the inner blood-retinal barrier (BRB) in the developing retina [1]. Retinal
41 angiogenesis is tightly coordinated with the maturation of the BRB properties by endothelial cells (ECs),
42 through the presence of tight-junctions (TJ) that limit paracellular permeability between ECs, specialized
43 transporters to facilitate bidirectional transport of nutrients, and suppression of transcytosis that reduces
44 transcellular EC permeability [2,3]. Although multiple signaling pathways operating in ECs, pericytes (PCs),
45 neuronal or glial cells have emerged as critical regulators of retinal angiogenesis and BRB maturation
46 [reviewed in [4]], it is unclear how distinct types of neuronal synaptic activities influence these processes,
47 and whether neurotransmitters act directly on ECs to mediate their effects. This is highly significant since
48 early loss of neurovascular coupling, impaired response of photoreceptors to light, gradual
49 neurodegeneration, gliosis and neuroinflammation are found prior to any obvious vascular pathologies in
50 diabetic retinopathy and other retinal disease [5-7]. Moreover, it has been postulated that diabetes-induced
51 changes in neurons and glial cells lead to vascular defects [8], yet the underlying mechanisms remain elusive.
52

53 Distinct types of neuronal activities are present in the postnatal mouse retina during angiogenesis
54 and BRB maturation **(Figure 1A)**. From birth to postnatal day (P) 10, starburst amacrine cells propagate
55 spontaneous cholinergic waves [9-11]. These cholinergic waves gradually subside and spontaneous
56 glutamatergic waves emerge from P10 to P14 [11-14]. The majority of neuronal activities in the mouse retina
57 from P14 onwards are mediated by light-dependent glutamatergic synaptic activity of photoreceptors, and
58 photoactivation of intrinsically-photosensitive retinal ganglion cells (ipRGCs) [reviewed in [4]]. However,
59 light activation of photoreceptors has been observed as early as P8 [13,15]. The superficial vascular plexus in
60 the retina develops between P0 - P8 [16] over the ganglion cell layer (GCL) synchronous with neuronal
61 activities from the cholinergic waves and photoactivation of ipRGCs. In contrast, the deep plexus
62 angiogenesis (P8 - P12) in the outer plexiform layer (OPL) [16] and BRB maturation (P6 - P18) span both

63 cholinergic and glutamatergic spontaneous waves, glutamatergic synaptic activity of photoreceptors as well
64 as photoactivation of ipRGCs [reviewed in [4]]. Few studies have addressed how neuronal activity regulates
65 retinal angiogenesis and BRB maturation in the developing retina. Photoactivation of both Opn4^{+} [17] and
66 Opn5^{+} [18] RGCs regulates angiogenesis in the retina. Pharmacological blockade of cholinergic waves before
67 P8 delays deep plexus angiogenesis and BRB maturation, suggesting an important role for cholinergic
68 activity in these processes [14]. However, the role of glutamatergic neuronal activities in retinal angiogenesis
69 and BRB maturation remains unclear, although it is the predominant type of neuronal activity when most
70 of the vascular development and BRB maturation occurs in the retina.
71
72 The Norrin/β-catenin signaling is critical for retinal angiogenesis and BRB maturation by inducing
73 stabilization and nuclear translocation of β-catenin. Genetic elimination of Norrin (ligand), Frizzled-4,
74 Lrp5/6, Tspan12 (receptors) and β-catenin in the mouse retina delays superficial vascular plexus
75 angiogenesis, induces loss of the deep plexus [19-23] and BRB integrity [24,25]. How Norrin expression and
76 endothelial Norrin/β-catenin signaling are related to the glutamatergic activities in the developing retina is
77 also unknown.
78
79 Using *in vivo* anatomical and functional characterizations of the vasculature, as well as single-cell
80 transcriptomic analyses and validation studies, we show that deep plexus angiogenesis and paracellular
81 BRB maturation are delayed in *Vglut1*$^{-/-}$ retinas that have reduced synaptic release of glutamate from
82 photoreceptors and bipolar cells [12]. In contrast, deep plexus angiogenesis is accelerated and paracellular
83 BRB matures precociously in *Gnat1*$^{-/-}$ retinas, where rod photoreceptors remain constitutively depolarized
84 due to the absence of α-Transducin, a Gα protein critical for phototransduction [26,27]. These phenotypes are
85 not due to abnormalities in neurovascular unit (NVU) assembly, aberrant specification of neuronal or glial
86 subtypes, or changes in the neuronal metabolic demand. Importantly, *Norrin* mRNA expression in the inner
87 nuclear layer (INL), and as a consequence endothelial Norrin/β-catenin signaling, are downregulated in

88 *Vglut1*$^{-/-}$ retinas, and upregulated in *Gnat1*$^{-/-}$ retinas. Pharmacological activation of endothelial Norrin/β-
89 catenin signaling in *Vglut1*$^{-/-}$ retinas rescues defects in both deep plexus angiogenesis and paracellular BRB
90 integrity. Our study elucidates a critical mechanism by which glutamatergic neuronal activities regulate
91 retinal angiogenesis and BRB maturation by modulating endothelial Norrin/β-catenin signaling in the
92 developing retina. These findings have important implications for development of potential interventions
93 in various neurovascular pathologies.
94
95 **RESULTS**
96 **Deep plexus angiogenesis is delayed in the *Vglut1*$^{-/-}$ retina.**
97 Photoreceptors release glutamate in the OPL in the dark and suppress glutamate release upon photon
98 capture [28]. The synaptic release of glutamate is dependent on vGluT1, a vesicular glutamate transporter [29].
99 Consequently, *Vglut1*$^{-/-}$ mice have reduced synaptic release of glutamate from photoreceptors and bipolar
100 cells **(Figure 1B)**[12]. To understand if extracellular glutamate levels affect retinal angiogenesis, we compared
101 the vascular growth in the superficial and deep plexuses between wild-type (WT) and *Vglut1*$^{-/-}$ retinas. Since
102 the central retina is developmentally more mature than the peripheral retina, we analyzed these two regions
103 separately **(Figure 1C)**. Although the vascular coverage of the retina in the superficial plexus was similar
104 in both genotypes at P8 and P10 **(Figure 1D, E, H, I)**, the vascular coverage of the retina in the deep plexus
105 and its branch-point density were reduced significantly in the P10 and P12 *Vglut1*$^{-/-}$ retinas **(Figure 1E-G,**
106 **J-M)**. By P14, however, the vascular coverage of the retina in the deep plexus was similar between the two
107 genotypes, although the branch-point density of the *Vglut1*$^{-/-}$ deep plexus was still significantly lower than
108 the WT **(Figure 1F, G, J-M)**. Importantly, these vascular abnormalities were consistent in both the central
109 and peripheral *Vglut1*$^{-/-}$ retinas (**Figure 1J-M**).
110
111 To understand the molecular mechanisms underlying these vascular phenotypes, we performed
112 single-cell RNA-sequencing analyses (scRNA-seq) of ECs that were dissociated from P10 WT and *Vglut1*$^{-}$

113 $^{/-}$ retinas and sorted for CD31 using fluorescence-activated cell sorting (FACS; **Figure S1A, B)**. The purity
114 of ECs was confirmed by uniform expression of EC markers [*Pecam1* (CD31) and *Cdh5* (VE-Cadherin)]
115 in the entire population, and absence of mural cell [*Pdgfrb* (PDGFRβ) and *Des* (Desmin)] and astrocyte
116 [*Gfap* and *Pdgfra*] markers **(Figure S1C)**. The majority of ECs isolated from either genotype were capillary
117 ECs (Mfsd2a+), as opposed to arterial or venous ECs **(Figure S1D)**, consistent with the predominant
118 distribution of this EC subtype in both the superficial and deep plexuses of the retina (the deep plexus has
119 only capillaries). ECs isolated from P10 WT and *Vglut1*$^{-/-}$ retinas clustered separately in the Uniform
120 Manifold Approximation and Projection (UMAP) plot based on differences in their transcriptomic
121 signatures **(Figure 2A; Tables S1, S2)**. Gene ontology (GO) analyses of the differentially expressed genes
122 (DEGs) between the two genotypes revealed that pathways related to "angiogenesis", "blood vessel
123 morphogenesis" and "cell proliferation" were downregulated in P10 *Vglut1*$^{-/-}$ compared to WT retinal ECs
124 **(Figure 2B; Tables S3, S5)**, consistent with the phenotypic analyses (**Figure 1**). In contrast, pathways
125 related to "cellular and protein metabolic processes" were upregulated in P10 *Vglut1*$^{-/-}$ compared to WT
126 retinal ECs **(Figure 2C; Tables S4)**. Expression levels of several pro-angiogenic genes [e.g. *Ptprb*, *Aplnr,*
127 *Unc5b* etc.], including two effectors of Norrin/β-catenin signaling [*Ctnnb1* (β-catenin) and *Lef1*], were
128 downregulated significantly in P10 *Vglut1*$^{-/-}$ compared to WT retinal ECs **(Figure 2D, F; Table S5)**. In
129 contrast, the majority of genes enriched in the deep plexus tip cells (D-tip cells) compared to the superficial
130 plexus tip cells (S-tip cells) [e.g. *Bsg*, *Rgcc*, *Plxnd1*, *Cdkn1a*, *Pde4b*, *Prcp*], as well as those enriched in D-
131 tip cells compared to all ECs [e.g. *Lamb1*, *Pcdh17*, *Adm*] [30] were upregulated in P10 *Vglut1*$^{-/-}$ compared to
132 WT retinal ECs **(Figure 2E, G; Table S6)**, indicative of delayed deep plexus angiogenesis at the
133 transcriptome level. To validate these molecular findings, we labeled proliferating cells with Ki67 in both
134 WT and *Vglut1*$^{-/-}$ retinas and assessed whether endothelial stalk cell proliferation was reduced in *Vglut1*$^{-/-}$
135 retinal ECs (**Figure 2H**) [31]. Consistent with the scRNA-seq data, there was a significant reduction in the
136 number of proliferating Ki67^{+} ECs in P12 *Vglut1*$^{-/-}$ retinal deep plexus compared to the WT **(Figure 2I, J)**,
137 while the number of apoptotic ECs (cleaved Caspase-3^{+}) was not significantly different **(Figure 2J)**.

138 Therefore, the delayed angiogenesis in *Vglut1*$^{-/-}$ retinal deep plexus is due, in part, to reduced EC
139 proliferation. Consistent with the scRNA-seq data, we also observed numerous Dll4^{+} tip cells [32,33] in the
140 leading edge of the *Vglut1*$^{-/-}$ deep plexus at P12, while the WT deep plexus was completely vascularized at
141 this stage **(Figure 2K, L)**. Thus, angiogenesis (EC proliferation) is delayed and the number of endothelial
142 tip cells is increased in the deep, but not superficial, plexus of *Vglut1*$^{-/-}$ retinas lacking extracellular
143 glutamate release by neurons.
144
145 **Deep plexus vessels are poorly perfused in the *Vglut1*$^{-/-}$ retina.**
146 Next, we asked if the deep plexus vessels are polarized and function normally in the *Vglut1*$^{-/-}$ retinas.
147 We stained blood vessels with Podocalyxin, which labels the apical (luminal) side of ECs, and is a marker
148 for endothelial apical-basal polarity **(Figure 3A)** [34]. Compared to the WT, Podocalyxin coverage of the
149 deep plexus vessels was significantly reduced in *Vglut1*$^{-/-}$ retinas at both P10 and P14 **(Figure 3B, C-E)**,
150 suggesting that EC polarity is abnormal in the deep vascular plexus. Next, we examined whether deep
151 plexus vessels are perfused normally in *Vglut1*$^{-/-}$ retinas. We performed intracardiac injection of
152 fluorescently-labeled Lectin and analyzed its binding to the retinal vasculature as a readout of perfusion.
153 By P14, the entire OPL in *Vglut1*$^{-/-}$ retinas is vascularized **(Figure 1)**. However, the fraction of Lectin^{+}
154 perfused blood vessels was significantly lower in the deep plexus of P14 *Vglut1*$^{-/-}$ compared to the WT
155 retinas **(Figure 3C, F)**. These data demonstrate that, although the deep plexus is fully formed by P14 in the
156 *Vglut1*$^{-/-}$ retinas (**Figure 1F, G**), EC polarity and vessel perfusion remain abnormal.
157
158 **Paracellular BRB maturation is impaired in the *Vglut1*$^{-/-}$ retina.**
159 Next, we asked if diminished glutamate release from photoreceptors and bipolar cells affects BRB
160 maturation. During retinal development, the transcellular (caveolae-mediated) BRB matures by P10 [35]
161 whereas the paracellular (tight junction-mediated) BRB does not mature until P18 [36] **(Figure 4A)**. We
162 therefore injected intravenously biocytin-tetramethylrhodamine (biocytin-TMR, 870 Da) tracer in WT and

163 *Vglut1*$^{-/-}$ mice at P10 and P14 and quantified its leakage in the retina as a functional readout of paracellular
164 BRB maturation **(Figure 4B)** [36,37]. Biocytin-TMR leakage (area and intensity) was higher in the *Vglut1*$^{-/-}$
165 compared to the WT retinas at both time points **(Figure 4C-I)**. Importantly, these patterns were consistent
166 in both the central and peripheral retina, and the superficial and deep plexuses. Consistent with a delay in
167 BRB maturation, scRNA-seq analyses revealed reduced transcript levels for most "BRB maturation genes"
168 in P10 *Vglut1*$^{-/-}$ compared to WT retinal ECs. These include tight junction-associated genes [*Cldn5*
169 (Claudin-5) and *Tjp1* (ZO-1)], transporters [*Slc7a5* (Lat1), *Slc2a1* (Glut1) etc.,] and effectors of Norrin/β-
170 catenin signaling [*Ctnnb1* and *Lef1*] **(Figure 4J, K; Table S7)**. Surprisingly, transcript levels for *Ocln*
171 (Occludin; tight junction protein), vBM proteins (Collagen IV, Laminin), BBB transcription factors (e.g.
172 *Foxq1*, *Foxf2*, *Zic3* etc.), or caveolar-related transport (*Cav-1*, *Cav-2*, *Cavin-1*, *Mfsd2a*) genes were
173 unaffected in P10 *Vglut1*$^{-/-}$ retinal ECs **(Tables S2, S7)**.
174
175 We validated the scRNA-seq findings for several tight junction proteins in the *Vglut1*$^{-/-}$ retina.
176 Consistent with the scRNA-seq data, there was a significant reduction in Claudin-5 and ZO-1 protein
177 localization to EC junctions at P14 *Vglut1*$^{-/-}$ compared to the WT retina in both the superficial and deep
178 plexuses by immunofluorescence (**Figure 4L-O**). Importantly, these phenotypes were not caused by
179 abnormalities in the NVU assembly, as mural cell (PDGFRβ^{+}), glial endfeet (Aquaporin-4; Aqp-4^{+}) and
180 vascular basement membrane (vBM; Laminin) coverage of retinal blood vessels were comparable between
181 the two genotypes **(Figure S2)**.
182
183 We next asked whether the lack of glutamate release by neurons affects the maturation of the
184 transcellular BRB properties. We injected intravenously albumin-Alexa594 (MW= 60kDa), a protein that
185 crosses the BRB primarily through a transcellular route [36] into P10 WT and *Vglut1*$^{-/-}$ mice and assessed its
186 extravasation into the retina. The tracer was largely confined within the blood vessels and its intensity in
187 the parenchyma was very low and identical between the two genotypes **(Figure S3A, B)**. In addition, there

188 was no difference in endogenous serum IgG leakage between P10 WT and *Vglut1*$^{-/-}$ retinas **(Figure S3C)**.
189 These functional studies are consistent with the scRNA-seq data showing no change in *Mfsd2a* (a gene
190 required for suppression of transcellular BRB permeability [35]) transcript levels between the two genotypes
191 **(Tables S2, S7)**. In addition, PLVAP expression, a component of the diaphragms of EC fenestrae normally
192 found in the immature BRB and peripheral ECs [38], was absent in retinal ECs from both genotypes **(Figure**
193 **S3D)** despite a slight downregulation in *Plvap* mRNA in P10 *Vglut1*$^{-/-}$ retinal ECs by scRNA-seq **(Figure**
194 **4J; Table S7)**. Similarly, immunofluorescence analysis showed no difference in retinal EC expression of
195 Caveolin-1 and Mfsd2a, two critical proteins responsible for regulating EC transcellular permeability
196 [4,35,39,40], between the two genotypes **(Figure S3E, F).** Thus, paracellular, but not transcellular, BRB
197 maturation is delayed in both the superficial and deep plexuses of *Vglut1*$^{-/-}$ retinas with decreased
198 extracellular glutamate **(Figure S3G)**.
199
200 **BRB maturation is accelerated in the absence of cholinergic waves due to an early onset of**
201 **glutamatergic activities.**
202 During development, the cholinergic waves persist beyond P10 in the *Vglut1*$^{-/-}$ retina lacking
203 glutamatergic neuronal activities [12]. Conversely, the glutamatergic waves begin earlier (P8) than usual (P10)
204 in the *Chrnb2*$^{-/-}$ retina where the cholinergic waves are abolished (**Figure 5A**) [11]. Recently it was reported
205 that pharmacological blockade of cholinergic waves before P8 delays deep plexus angiogenesis and BRB
206 maturation, suggesting a critical role for the cholinergic waves in promoting these processes in the
207 developing retina [14]. In contrast, our phenotypic analysis of the *Vglut1*$^{-/-}$ retinal vasculature implies that the
208 cholinergic waves are not sufficient to induce paracellular BRB maturation since it is very delayed in the
209 *Vglut1*$^{-/-}$ retina throughout P14 (**Figure 4**). To test this hypothesis, we examined angiogenesis and the
210 paracellular BRB integrity in the *Chrnb2*$^{-/-}$ retina where cholinergic waves are abolished and glutamatergic
211 waves begin earlier (P8) than usual [11] **(Figure 5A)**. At P7, before the onset of glutamatergic waves in the
212 *Chrnb2*$^{-/-}$ retina, there was no difference in the vascularized area of the superficial plexus **(Figure 5B, C),**

213 and biocytin-TMR leakage **(Figure 5D-F)** between WT and *Chrnb2*$^{-/-}$ retinas. In contrast, there was less
214 biocytin-TMR leakage in the parenchyma **(Figure 5J-L),** and increased Claudin-5 coverage of blood
215 vessels **(Figure 5M, N)** in the P10 *Chrnb2*$^{-/-}$ retina compared to the WT. However, vascular coverage in
216 either the superficial or deep plexus was not significantly different between P10 WT and *Chrnb2*$^{-/-}$ retinas
217 **(Figure 5G-I)**. These data are consistent with the idea that the earlier onset of glutamatergic waves in the
218 *Chrnb2*$^{-/-}$ retina is sufficient to promote a precocious BRB maturation, but does not affect deep plexus
219 angiogenesis. Moreover, they demonstrate that glutamatergic neuronal activities, but not the cholinergic
220 waves, are the primary drivers of paracellular BRB maturation in the developing retina.
221
222 **Deep plexus angiogenesis and paracellular BRB maturation are accelerated in the *Gnat1*$^{-/-}$ retina.**
223 To further evaluate the effect of excess glutamate release by retinal neurons, we examined the retinal
224 vascular phenotypes in mice lacking α−Transducin. Phototransduction by rod photoreceptors is a complex
225 cascade, dependent in part on the Gα subunit, Transducin 1 (*Gnat1*). *Gnat1*$^{-/-}$ rod photoreceptors remain
226 constitutively depolarized [26,27] leading to increased glutamate release from rods **(Figure 6A, B)**. To
227 understand how excess glutamate release by rod photoreceptors affects retinal angiogenesis, we compared
228 the vascular growth of the superficial and deep plexuses between the WT and *Gnat1*$^{-/-}$ retinas. While the
229 vascular coverage of the retina in the superficial plexus was similar between the two genotypes at P10
230 **(Figure 6C, D)**, both the vascular coverage of the retina in the deep plexus, and its branch-point density
231 were significantly increased in the *Gnat1*$^{-/-}$ retina **(Figure 6E-J)**. However, the angiogenesis phenotype was
232 transient, and by P14 there was no difference between the two genotypes **(Figure 6F, G, I, J; Figure S4A)**.
233 Importantly, these patterns were similar in both central and peripheral retina. Consistent with an accelerated
234 deep plexus angiogenesis in the P10 *Gnat1*$^{-/-}$, there was also increased EC proliferation (Ki67^{+} ECs) in
235 mutant deep vascular plexus compared to the WT **(Figure 6K, L)**.
236

237 Next, we asked whether excess glutamate release by rod photoreceptors affects paracellular BRB
238 maturation. Biocytin-TMR leakage area and fluorescence intensity were reduced in *Gnat1*$^{-/-}$ compared to
239 the WT retinas in both central and peripheral retinas and superficial and deep plexuses at P10 and P14
240 **(Figures 6M-O; S4B-D)**. Consistent with the functional data, there was a significant increase in Claudin-5
241 protein localization at BRB tight junctions in the P10 *Gnat1*$^{-/-}$ retina compared to the WT **(Figure 6P-R)**.
242 In summary, retinal deep plexus angiogenesis is accelerated and paracellular BRB integrity is precociously
243 mature when there is excess glutamate release by the rods.
244
245 To address whether aberrant specification of neuronal subtypes or Müller glia in either *Vglut1*$^{-/-}$ or
246 *Gnat1*$^{-/-}$ retinas may be responsible for the vascular phenotypes seen in these mutants, we immunolabelled
247 and quantified the number of neuronal subtypes and Müller glia. There was no significant difference in the
248 number of ganglion cells [NeuN^{+} [41,42]], amacrine (except for a slight reduction in the *Vglut1*$^{-/-}$ retina) and
249 horizontal cells [Calbindin^{+} [43]], photoreceptors [measured by outer nuclear layer (ONL) thickness] among
250 the three genotypes **(Figure S5A-I)**. Similarly, the number of Sox9^{+} Müller glia [44,45] was similar among
251 WT, *Vglut1*$^{-/-}$ and *Gnat1*$^{-/-}$ retinas **(Figure S5J, K)**. Importantly, altered levels of extracellular glutamate
252 did not trigger Müller cell gliosis in *Vglut1*$^{-/-}$ and *Gnat1*$^{-/-}$ retinas, as there was no upregulation of GFAP
253 expression [a marker of gliosis [46,47]] in Müller glia processes spanning multiple retinal layers (**Figure S5L**).
254 GFAP expression was only detected in retinal astrocytes over the GCL (colocalized with PDGFRα) **(Figure**
255 **S5L, M)**. Therefore, the angiogenesis and BRB phenotypes seen in *Vglut1*$^{-/-}$ and *Gnat1*$^{-/-}$ retinas are not
256 caused by defects in neuronal and glial cell type specification.
257
258 Finally, we examined whether cholinergic, GABAergic and dopaminergic neuronal populations are
259 altered in mutant retinas with abnormal glutamatergic activities which may indirectly affect vascular
260 development. There was no difference in the number of ChAT^{+} (cholinergic), GAD67^{+} (GABAergic) and
261 Tyrosine Hydroxylase (TH)$^{+}$ (dopaminergic) neurons between WT, *Vglut1*$^{-/-}$ and *Gnat1*$^{-/-}$ retinas **(Figure**

262 **S6A, B)**. Overall, our data show that changes in extracellular glutamate does not affect neuronal or glial
263 subtypes specification or neurons involved in other types of neurotransmission.
264
265 **Neurons and Müller glia in the inner nuclear layer of the retina respond to altered levels of**
266 **extracellular glutamate.**
267 To understand how extracellular glutamate affects retinal angiogenesis and paracellular BRB
268 maturation, we examined several parameters that could influence these processes. First, we asked whether
269 glutamate acts directly on retinal ECs. Our scRNA-seq analyses of P10 and P14 WT retinal ECs showed
270 that neither ionotropic (*Grin1*, *Grin2b*, *Grin2d*, *Gria1*), nor metabotropic (*Grm3*, *Grm5*, *Grm6*, *Grm7*,
271 *Grm8*) glutamate receptor subunit transcripts are expressed in developing retinal ECs **(Figure S6C).**
272 Analysis of a previously published scRNA-seq database of all cell types from the P14 retina [48] also
273 confirmed our findings that glutamate receptor subunit transcripts are not expressed in P14 retinal ECs.
274 Thus, glutamate cannot act directly on developing retinal ECs. In contrast, ionotropic and metabotropic
275 glutamate receptor subunit mRNAs are expressed by the inner nuclear layer (INL) neurons and Müller glia
276 **(Figure S6D)**, suggesting that extracellular glutamate could act on INL neurons and Müller glia.
277
278 To examine whether altered levels of extracellular glutamate are sensed by Müller glia in *Vglut1*$^{-/-}$
279 and *Gnat1*$^{-/-}$ retinas, we initially measured mean fluorescence intensity of glutamine synthetase (GS), an
280 enzyme that coverts glutamate to glutamine, and the Glutamate Aspartate Transporter [GLAST, excitatory
281 aminoacid transporter 1 (EAAT-1)] from immunofluorescence staining. These proteins are known to be
282 upregulated in Müller glia exposed to excess extracellular glutamate [49,50]. GS and GLAST protein levels
283 were downregulated in *Vglut1*$^{-/-}$, and upregulated in *Gnat1*$^{-/-}$ retinas, compared to the WT retinas **(Figure**
284 **7A-D)**. To determine whether altered levels of extracellular glutamate are sensed by neurons in *Vglut1*$^{-/-}$
285 and *Gnat1*$^{-/-}$ retinas, we measured Glutamate Transporter 1 protein levels [GLT-1, or excitatory aminoacid
286 transporter 1 (EAAT-2)]. This transporter is expressed primarily in retinal neurons [51], and its expression is

287 regulated by extracellular glutamate [52]. GLT-1 expression in INL neurons was downregulated in the *Vglut1*-
288 /-, and upregulated in the *Gnat1*$^{-/-}$ retinas, compared to the WT **(Figure 7E-F)**. These data confirm that
289 Müller glia and INL neurons respond to abnormal extracellular glutamate levels in *Vglut1*$^{-/-}$ or *Gnat1*$^{-/-}$
290 retinas.
291
292 **Retinal metabolic demand, hypoxia and VEGF-A signaling are not affected in the *Vglut1*$^{-/-}$ retina.**
293 Since Müller glia and INL neurons respond to changes in extracellular glutamate levels, we asked
294 whether neuronal metabolic demand is also affected in *Vglut1*$^{-/-}$ and *Gnat1*$^{-/-}$ retinas, as alterations in
295 neuronal metabolic demand trigger vascular abnormalities [reviewed in [4]]. We examined Hexokinase-2
296 (HK2) and Pyruvate Kinase M-2 (PKM2) protein levels by Western blotting since they are key glycolytic
297 enzymes of neuronal metabolism readout [53]. The levels of these enzymes were similar among P10 WT,
298 *Gnat1*$^{-/-}$ and *Vglut1*$^{-/-}$ retinas **(Figure S7A-L)**. Thus, alterations in extracellular glutamate levels caused by
299 genetic perturbations in glutamate release from neurons do not affect expression of key enzymes for the
300 neuronal metabolism in the retina.
301
302 Neuronal-derived VEGF-A is critical for nervous system function [54] and VEGF-A signaling is a
303 major regulator of retinal angiogenesis [14,55], prompting us to examine whether VEGF-A levels change in
304 *Vglut1*$^{-/-}$ and *Gnat1*$^{-/-}$ retinas. VEGF-A protein levels measured with Western blotting were not different
305 among WT, *Vglut1*$^{-/-}$ and *Gnat1*$^{-/-}$ retinas **(Figure S7M-P)**. These results are also consistent with our
306 scRNA-seq data showing no changes in transcripts for VEGF-A signaling components [*Nr4a2*, *Egr3*,
307 *Igfbp3*, *Hlx1*, *Crem*, *Per1*, *Mef2c*, *Thbd*, *Ndrg1*, *Dnajb9*, *Mycn* [56]] in *Vglut1*$^{-/-}$ retinal ECs **(Figure S7Q;**
308 **Table S2)**. Since VEGF-A expression depends on tissue hypoxia [57], we measured retinal hypoxia with a
309 hypoxyprobe, Pimonidazole [58,59]. Consistent with no change in VEGF-A protein and downstream target
310 transcript levels, there was no difference in tissue hypoxia between *Vglut1*$^{-/-}$ and WT retinas **(Figure S7R,**

311 **S)**. Therefore, the vascular phenotypes observed in mutants with altered extracellular glutamate are not due
312 to changes in VEGF-A signaling and hypoxia.
313
314 **Extracellular glutamate levels affect Norrin expression in retinal neurons and Müller glia and as a**
315 **consequence endothelial Norrin/β-catenin signaling.**
316 Our scRNA-seq analyses showed that transcript levels for two Norrin/β-catenin signaling effectors
317 (*Ctnnb1* and *Lef1*), essential for angiogenesis and BRB maturation, were downregulated in P10 *Vglut1*$^{-/-}$
318 compared to WT retinal ECs **(Figures 2D, F; 4J)**. Among seven key transcription factors (*Foxf2*, *Foxl2*,
319 *Foxq1*, *Lef1*, *Ppard*, *Zfp551* and *Zic3*) required for BBB maturation [60], only *Lef1* was downregulated
320 significantly in P10 *Vglut1*$^{-/-}$ retinal ECs, suggesting a specific effect on Norrin/β-catenin signaling. To
321 address changes in Norrin/β-catenin signaling, we examined *Norrin* (*Ndp*) mRNA expression in *Vglut1*$^{-/-}$
322 and *Gnat1*$^{-/-}$ retinas by fluorescent *in situ* hybridization (FISH). *Norrin* mRNA expression was reduced in
323 the INL of P10 *Vglut1*$^{-/-}$ retinas, and upregulated in the INL of P10 *Gnat1*$^{-/-}$ retinas, compared to the WT
324 **(Figure 7G, H)**. The upregulation of *Norrin* mRNA persisted in the INL of *Gnat1*$^{-/-}$ retinas through P14
325 **(Figure S4E)**. Consistent with our data, analysis of a previously published scRNA-seq database [48]
326 demonstrated that INL neurons (horizontal cells and a subset of amacrine and bipolar cells) and Müller glia
327 express high levels of *Norrin* mRNA and glutamate transporters [*Slc1a2* (GLT-1) and *Slc1a3* (GLAST)]
328 respectively [48] **(Figure 7I)**. These transcriptional data and the response of the INL neurons and Müller glia
329 to extracellular glutamate in the *Vglut1*$^{-/-}$ and *Gnat1*$^{-/-}$ retinas (**Figure 7A-F**) suggest that glutamate may act
330 directly on Müller glia and INL neurons to induce *Norrin* mRNA expression.
331
332 To test whether glutamate can induce *Norrin* mRNA expression in Müller glia and INL neurons, we
333 performed *ex vivo* organotypic cultures of P10 WT retinas in the presence or absence of glutamate
334 (0.01mM) and measured *Norrin* mRNA expression in the INL by FISH (fluorescence intensity) after 6 and
335 12 hours in culture (**Figure 7J**). *Norrin* mRNA expression in the INL was upregulated after 6 hours of

336 glutamate exposure, although it was not statistically significant (p=0.16; **Figure 7K, L)**. By 12 hours,
337 *Norrin* mRNA levels in the INL were upregulated significantly with glutamate compared to media alone
338 **(Figure 7K, M)**. Therefore, glutamate induces *Norrin* mRNA expression in Müller glia and INL neurons.
339
340 Glutamate-mediated induction of *Norrin* mRNA expression in Müller glia and INL neurons may be
341 regulated through glutamate uptake via GLAST and GLT-1. To test this directly, we performed *ex vivo*
342 organotypic cultures of P10 WT retinas with or without glutamate and TFB-TBOA, a pharmacological
343 inhibitor of GLAST and GLT-1[61-63] **(Figure 7J)**. *Norrin* mRNA expression in the INL was downregulated
344 significantly with glutamate and TFB-TBOA compared to glutamate alone conditions after 6 and 12 hours
345 in culture **(Figure 7K-M)**. Importantly, TFB-TBOA alone did not alter *Norrin* mRNA levels in the INL
346 compared to the media alone **(Figure 7K, M)**, suggesting that TFB-TBOA did not have any non-specific
347 effect on *Norrin* mRNA expression. Based on these pharmacological data, we conclude that glutamate
348 uptake by GLAST and GLT-1 likely induces *Norrin* mRNA expression in both Müller glia and INL
349 neurons.
350
351 Next, we examined Norrin/β-catenin signaling activation in *Vglut1*$^{-/-}$ and *Gnat1*$^{-/-}$ retinal ECs. We
352 immunolabeled P14 WT, *Vglut1*$^{-/-}$ and *Gnat1*$^{-/-}$ retinal sections with Lef1 and quantified the number of
353 Lef1^{+} ECs in both the superficial and deep plexuses. There were significantly fewer Lef1^{+} ECs in the *Vglut1*$^{-}$
354 $^{/-}$ retina and significantly higher in the *Gnat1*$^{-/-}$ retina compared to the WT **(Figure 8A, B)**. These data
355 suggest that angiogenesis and BRB phenotypes in *Vglut1*$^{-/-}$ and *Gnat1*$^{-/-}$ retinas are likely driven by altered
356 Norrin/β-catenin signaling.
357
358 **Activation of endothelial Norrin/β-catenin signaling restores retinal angiogenesis and BRB deficits in**
359 ***Vglut1*$^{-/-}$ mice.**

360 If angiogenesis and BRB phenotypes observed in *Vglut1*$^{-/-}$ and *Gnat1*$^{-/-}$ retinas are driven by altered
361 endothelial Norrin/β-catenin activity, then activation of Norrin/β-catenin signaling in retinal ECs should
362 rescue angiogenesis and BRB phenotypes in *Vglut1*$^{-/-}$ retinas. We injected intraperitoneally either BIO, a
363 compound that activates Wnt (Norrin)/β-catenin signaling by inhibiting GSK-3β, or an inactive analog
364 MeBIO [64], in WT and *Vglut1*$^{-/-}$ mice between P6 - P8 and analyzed the vascular and BRB phenotypes in the
365 retina at P10. BIO-treatment significantly increased the number of Lef1^{+} ECs in the *Vglut1*$^{-/-}$ retina
366 compared to the MeBIO-treated *Vglut1*$^{-/-}$ retina, whereas MeBIO administration had no effect on endothelial
367 Lef1 [there were significantly fewer Lef1^{+} ECs in the MeBIO-treated *Vglut1*$^{-/-}$ compared to the MeBIO-
368 treated WT retina (**Figure 8C, D**)]. Importantly, there were no Lef1^{+} nuclei outside the vasculature with
369 either treatment **(Figure 8C, D)**. Therefore, BIO-treatment activated Norrin/β-catenin signaling specifically
370 in *Vglut1*$^{-/-}$ retinal ECs.
371
372 BIO-treatment significantly increased vascular coverage by the deep plexus in *Vglut1*$^{-/-}$ retina to
373 levels comparable to MeBIO-treated WT retinas **(Figure 8E-G)**. However, the vascular coverage of the
374 deep plexus was significantly lower in the MeBIO-treated *Vglut1*$^{-/-}$ retina compared to the MeBIO-treated
375 WT retina, consistent with no effect of MeBIO on endothelial Norrin/β-catenin activation (**Figure 8C, D**).
376 Similarly, BIO-treatment significantly decreased biocytin-TMR leakage area and intensity in the *Vglut1*$^{-/-}$
377 retina similar to those observed in MeBIO-treated WT levels **(Figure 8H-K),** whereas Me-BIO treatment
378 had no effect [biocytin-TMR leakage area and intensity were significantly higher in the MeBIO-treated
379 *Vglut1*$^{-/-}$ retina compared to the MeBIO-treated WT retina (**Figure 8H-K**)]. Interestingly, although BIO
380 administration in WT mice decreased modestly biocytin-TMR leakage in the retina compared to the MeBIO
381 administration **(Figure S8C-E)**, the vascular coverage of the deep plexus was reduced significantly in the
382 BIO-treated compared to the MeBIO-treated WT retina **(Figure S8A, B)**. These data are consistent with
383 our previous findings that endothelial Norrin/β-catenin activation needs to be finely tuned for proper deep

384 plexus angiogenesis and BRB maturation in the developing retina [36]. In summary, activation of endothelial
385 Norrin/β-catenin signaling was sufficient to rescue angiogenesis and BRB phenotypes in the *Vglut1*$^{-/-}$ retina.
386
387 Taken together, our data demonstrate that glutamate released by neurons regulates retinal
388 angiogenesis and paracellular BRB integrity by modulating Norrin expression in retinal neurons and Müller
389 glia and endothelial Norrin/β-catenin signaling activation.
390
391 **DISCUSSION**
392 It is well established that neuronal and vascular development in the CNS, including the retina, are
393 interdependent. Axonal growth and sprouting angiogenesis use multiple similar guidance cues [65,66]. CNS
394 vascular growth is also regulated by the neuronal metabolism [43,67,68], as CNS is the most metabolically
395 active organ system in the body. CNS neurons use a multitude of neurotransmitters such as glutamate, acetyl
396 choline, dopamine and GABA. However, it is unclear whether specific types of neuronal activities and
397 neurotransmitters affect CNS vascular growth. A recent study suggested that dopaminergic activities of
398 ganglion cells regulate retinal superficial plexus angiogenesis [69]. Cholinergic waves propagated by starburst
399 amacrine cells have also been implicated in the development of retinal deep plexus vessels and BRB
400 maturation [14]. While glutamate is the predominant neurotransmitter in the retina during vascular
401 development and in adulthood [70], nothing is known about whether glutamatergic neuronal activities regulate
402 retinal angiogenesis and BRB maturation. Our study elucidates this critical missing step that links
403 glutamatergic neuronal activities with vascular development and maturation in the retina - a process that
404 may also be relevant for several retinal disease. Below, we discuss: a) the role of glutamate in angiogenesis
405 and barriergenesis, b) the signaling pathways that function downstream of glutamate to promote these
406 processes, and c) the relevance for the disease.
407

408 In our study, we used three mouse models to address the role of glutamate in angiogenesis and
409 barriergenesis: a) *Vglut1*$^{-/-}$, where retinal photoreceptors and bipolar cells fail to release glutamate into the
410 synaptic cleft, b) *Gnat1*$^{-/-}$, where depolarized rod photoreceptors release excess glutamate into the synaptic
411 cleft, and c) *Chrnb*2$^{-/-}$, where cholinergic waves are abolished but glutamatergic waves begin at P8 instead
412 of P10. We found that deep plexus angiogenesis and paracellular BRB maturation in the retina are critically
413 linked to the extracellular glutamate levels. These processes are delayed in *Vglut1*$^{-/-}$ retinas, where neurons
414 fail to release glutamate. In contrast, deep plexus angiogenesis and paracellular BRB maturation are
415 accelerated in *Gnat1*$^{-/-}$ retinas, where constitutively depolarized rods release excessive glutamate. Although
416 the deep plexus angiogenesis, which occurs from P8-P12, was affected in all mutant mouse models, the
417 superficial plexus angiogenesis (P0-P8) was unperturbed. This is likely because the superficial plexus is
418 fully formed by P8, before the onset of glutamatergic neuronal activities in the mouse retina. This
419 developmental time course can also explain why treatment with 2-amino-4-phosphonobutyrate, a
420 compound that blocks glutamatergic waves, from P3- P7 did not affect retinal angiogenesis in a previous
421 study [14], because the treatment was performed before the onset of glutamatergic waves in the developing
422 mouse retina. Similarly, we found that the transcellular, but not paracellular BRB, was also not affected in
423 the *Vglut1*$^{-/-}$ retina. This is consistent with previous studies showing that transcellular BRB in the mouse
424 retina is fully mature by P10 [3], whereas paracellular BRB does not fully mature until P18 [36]. Thus, it is
425 conceivable that glutamatergic neuronal activities kick in too late to affect the maturation of the transcellular
426 BRB, but have enough time to influence the maturation of the paracellular BRB.
427
428 Interestingly, *Vglut1*$^{-/-}$ retinas lacking glutamatergic neuronal activities show persistent cholinergic
429 waves beyond P10 [12]. Since deficits in the deep plexus angiogenesis and paracellular BRB integrity persist
430 in the *Vglut1*$^{-/-}$ retina throughout P14, our data suggest that the cholinergic waves are not sufficient to
431 promote deep plexus angiogenesis and paracellular BRB maturation. In contrast, paracellular BRB is
432 precociously mature in the *Chrnb2*$^{-/-}$ retina where cholinergic waves are abolished and glutamatergic waves

433 begin earlier (P8) than usual [11]. Overall these data indicate that glutamatergic neuronal activities are the
434 primary driver of paracellular BRB maturation. We were not able to extend our studies beyond P14 in
435 *Vglut1*$^{-/-}$ mice, as the pups die around P15 [71]. Notably, the vascular phenotypes, albeit opposite, were more
436 severe in the *Vglut1*$^{-/-}$ retina compared to the *Gnat1*$^{-/-}$ retina. This is likely because glutamate release is
437 abolished from both bipolar cells and photoreceptors (rods and cones) in the *Vglut1*$^{-/-}$ retina [12]. In contrast,
438 only depolarized rod photoreceptors release excess glutamate in the *Gnat1*$^{-/-}$ retina [26,27]. This may likely
439 explain why the vascular phenotypes are less prominent in the P10 *Gnat1*$^{-/-}$ retina, and possibly why the
440 angiogenic phenotype (but not BRB phenotype) in the *Gnat1*$^{-/-}$ retina normalizes to wild-type levels by P14.
441

442 How does extracellular glutamate trigger angiogenesis and BRB maturation in the developing
443 retina? It is possible that the vascular phenotypes in *Vglut1*$^{-/-}$ and *Gnat1*$^{-/-}$ retinas could be due to alterations
444 in either neuronal numbers which have been shown to affect retinal angiogenesis by titrating the level of
445 available pro-angiogenic factor VEGF-A [55]. However, we did not observe any significant differences in the
446 numbers of neuronal subtypes between WT, *Vglut1*$^{-/-}$ and *Gnat1*$^{-/-}$ retinas. While there was a slight decrease
447 in calbindin-labelled amacrine cells in the *Vglut1*$^{-/-}$ retina, identified classes of amacrine cells, including
448 cholinergic, GABAergic and dopaminergic neurons, were unaffected in these mutant retinas. These data
449 suggest that angiogenesis and BRB phenotypes in *Vglut1*$^{-/-}$ and *Gnat1*$^{-/-}$ retinas are not caused by alterations
450 in neuronal numbers. Metabolic demand of retinal neurons also modulates angiogenesis [43,67,68]. However,
451 the expression levels of HK2 and PKM2, two key glycolytic enzymes that are readouts of photoreceptor
452 cell metabolism [53], were unaffected in both P10 *Vglut1*$^{-/-}$ and *Gnat1*$^{-/-}$ retinas compared to the WT, in spite
453 of the prominent vascular phenotypes in these mutant retinas at this developmental stage. Similarly, retinal
454 hypoxia as well as VEGF-A expression levels were also unaffected in both P10 *Vglut1*$^{-/-}$ and *Gnat1*$^{-/-}$ retinas
455 compared to the WT. These data suggest that angiogenesis and BRB maturation abnormalities seen in these
456 mutant retinas are not due to alterations in neuronal numbers and neuronal metabolic demand or VEGF-A
457 signaling.

458

459 Our data demonstrate that *Norrin* mRNA expression and endothelial Norrin/β-catenin activity are
460 downregulated in *Vglut1*$^{-/-}$ retinas and upregulated in *Gnat1*$^{-/-}$ retinas between P10-P14, and therefore are
461 likely regulated by the extracellular glutamate concentration. Consistent with these findings our scRNA-
462 seq analyses showed that expression levels of effectors of Norrin/β-catenin pathway [*Ctnnb1* and *Lef1*] are
463 downregulated in *Vglut1*$^{-/-}$ retinal ECs. However, *Norrin* mRNA is expressed in the retina before P10 [20],
464 and perturbation of Norrin/β-catenin signaling delays superficial plexus angiogenesis as early as P5 [20,25],
465 well before the onset of glutamatergic neuronal activity. Therefore, early (P5-P8) *Norrin* mRNA expression
466 in the retina, which is critical for superficial plexus angiogenesis, is likely regulated by a glutamate-
467 independent mechanism [48]. Our data in conjunction with a previous study [48] also suggest that *Norrin* mRNA
468 is expressed by several cell types in the developing retina including Müller glia and INL neurons (horizontal
469 cells and subsets of amacrine and bipolar cells). Using *ex vivo* organotypic cultures, we also show that
470 glutamate can directly induce *Norrin* mRNA expression in the Müller glia and INL neurons, and this occurs
471 via glutamate uptake by GLAST and GLT-1, two glutamate transporters expressed in Müller glia and INL
472 neurons. We used a high concentration of TFB-TBOA (GLAST and GLT-1 inhibitor) in our study in order
473 to ensure that glia- and neuron-mediated glutamate uptake is completely inhibited in our *ex vivo* culture
474 system. Importantly, the presence of TFB-TBOA in the media in the absence of glutamate did not
475 significantly alter *Norrin* mRNA expression compared to the retinas with neither glutamate nor TFB-TBOA
476 in the media, confirming that TFB-TBOA does not affect *Norrin* mRNA expression in the retina. Future
477 studies will elucidate the relative contribution of Müller glia- or INL neurons-derived Norrin, regulated by
478 glutamate, for the deep plexus angiogenesis and paracellular BRB maturation. Importantly,
479 pharmacological activation of endothelial Norrin/β-catenin signaling was sufficient to rescue both deep
480 plexus angiogenesis and paracellular BRB integrity in the *Vglut1*$^{-/-}$ retina, consistent with the idea that
481 Norrin/β-catenin signaling functions downstream of extracellular glutamate to promote these processes.
482 Our scRNA-seq data also show a slight downregulation of *Unc5b* in *Vglut1*$^{-/-}$ retinal ECs. Unc5b has been

483 shown to modulate Wnt/β-catenin signaling in CNS ECs [72], suggesting the possibility that the cross-talk
484 between these two pathways may be affected in *Vglut1*$^{-/-}$ retinal ECs. Interestingly, none of the downstream
485 targets of VEGF-A signaling was affected in *Vglut1*$^{-/-}$ retinal ECs at the transcriptome level. Thus, VEGF-
486 A signaling pathway does not appear to be regulated by glutamate in the developing retina.
487
488 Taken together our data suggest a new mechanism by which glutamatergic neuronal activity regulate
489 retinal angiogenesis and BRB maturation in the developing retina **(Figure 8L)**. We propose that
490 extracellular glutamate, released either during spontaneous glutamatergic waves or light-dependent
491 glutamatergic synaptic activity of photoreceptors from P8 onwards, signals to Müller glia and INL neurons.
492 Glutamate signaling induces Norrin mRNA and protein expression and secretion by Müller glia and INL
493 neurons. Norrin, in turn, activates endothelial Norrin/β-catenin signaling in ECs which promotes
494 angiogenesis in the deep plexus and paracellular BRB maturation in both superficial and deep plexuses of
495 the retina (**Figure 8L**). Our genetic data in *Vglut1*$^{-/-}$ (no glutamate release into the synaptic cleft), *Gnat1*$^{-/-}$
496 (excess glutamate release into the synaptic cleft) and *Chrnb*2$^{-/-}$ (early onset of the glutamatergic waves),
497 and the pharmacological rescue of *Vglut1*$^{-/-}$ phenotypes by activation of endothelial Norrin/β-catenin
498 signaling, are consistent with the proposed model that extracellular glutamate levels control deep plexus
499 angiogenesis and barriergenesis. Although, the exact mechanisms by which glutamate mediates these
500 effects are not fully clear, our single-cell RNA-seq data together with the published datasets [48] suggest that
501 glutamate cannot act directly on ECs as they do not express either ionotropic or metabotropic glutamate
502 receptor subunits or glutamate transporters. The published transcriptional data of the glutamate receptor
503 and transporter expression [48], and our analysis of the response of the INL cells (neurons and Müller glia) to
504 extracellular glutamate (i.e, changes in GS, GLAST, GLT-1 protein levels) in the *Vglut1*$^{-/-}$ and *Gnat1*$^{-/-}$
505 retinas, suggest that glutamate could directly act on Müller glia and INL neurons to induce *Norrin* mRNA
506 expression. These cells express subsets of ionotropic or metabotropic glutamate receptors and glutamate
507 transporters that make them exquisite sensors of extracellular glutamate levels. In addition, *Norrin* mRNA

508 is predominantly expressed by the INL cells during vascular development and maturation. Future studies
509 will address in more detail the molecular mechanisms by which glutamate affects Norrin expression in the
510 INL cells and specific contributions of INL cell-derived Norrin to angiogenesis and barriergenesis.
511
512 Structural and functional abnormalities in neurons or glial cells precede vascular pathologies in
513 multiple CNS neurological diseases with prominent vascular involvement, including those in the retina. For
514 example, in diabetic retinopathy there is an early loss of neurovascular coupling, impaired response of
515 photoreceptors to light, gradual neurodegeneration, gliosis and neuroinflammation before any observable
516 vascular pathologies [5-7]. Moreover, the early phases of either age-related macular degeneration, or retinitis
517 pigmentosa, characterized by changes in synaptic activity and metabolic deficits in Müller glia [73-75], may
518 also affect blood vessel function leading to neurodegeneration. Although vascular pathologies, including
519 aberrant angiogenesis and BRB breakdown, are found in diabetic retinopathy and proliferative
520 vitreoretinopathy that cause acquired adult blindness, as well as retinopathy of prematurity which leads to
521 blindness in premature infants [1,76-78], the molecular mechanisms that link neuronal or glial abnormalities
522 with vascular deficits remain elusive. Our findings not only extend our understanding of the molecular
523 mechanisms by which vascular development and homeostasis occurs in the CNS [reviewed in [4]] including
524 the role that neuronal activity plays in these processes both in the cortex [79] and retina [14,17,18], but also have
525 important implications to identify putative interventions to treat CNS neurovascular pathologies, including
526 those in the retina from diabetic retinopathy, retinitis pigmentosa to age-related macular degeneration.
527

528 **ACKNOWLEDGEMENTS**

529 We thank Dr. Vilas Menon (Columbia University Irving Medical Center) for his consultation on
530 computational analyses and Dr. Eduardo Solessio (Upstate Medical University, State University of New
531 York) for his consultation about *Gnat1*$^{-/-}$ retinal physiology. S.B., S.S., and D.A. are supported by grants
532 from the National Eye Institute (R01EY033994 and K99EY033909), National Heart Lung and Blood

533 Institute (R61HL159949, R33HL159949), National Institute of Aging (RF1AG078352), National Institute
534 of Neurological Disorders and Stroke (R21 NS130265), the National Multiple Sclerosis Society (RG-1901-
535 33218) and in part by a gift donation. W.J.B. and G.B. are supported by grants from the National Eye
536 Institute (R01 EY033994 and R21 EY034696) and in part by funds from an unrestricted grant from
537 Research to Prevent Blindness to the Department of Ophthalmology and Visual Sciences, Upstate Medical
538 University.

539

540 **AUTHOR CONTRIBUTIONS**

541 Conceptualization: S.B., W.J.B., D.A.; Methodology: S.B., D.A., G.B.; Software: S.S.; Validation: S.B.,
542 G.B; Formal analysis: S.B., S.S., G.B., P.A., D.J.; Investigation: S.B., S.S., G.B.; Resources: W.J.B., D.A.;
543 Data curation: S.B., S.S., G.B.; Writing - original draft: S.B., D.A.; Writing - review & editing: S.B., S.S.,
544 G.B., W.J.B., D.A.; Visualization: S.B.; Supervision: W.J.B., D.A., Project administration: D.A., Funding
545 acquisition: W.J.B., D.A.

546

547 **DECLARATION OF INTEREST**

548 The authors declare no competing or financial interests.

549 **STAR ★ METHODS**

550 Detailed methods are provided in the online version of this paper and include the following:

551 KEY RESOURCES TABLE

552 RESOURCE AVAILABILITY

553 - Lead contact

554 - Materials availability

555 - Data and code availability

556 EXPERIMENTAL MODEL AND SUBJECT DETAILS

557 - Mice

558 METHOD DETAILS

559 - Immunohistochemistry

560 - Western blot

561 - Antibodies

562 - *In situ* hybridization

563 - Barrier permeability assays

564 - Vessel perfusion assay

565 - Hypoxia measurement

566 - Retinal endothelial cell isolation

567 - Retinal organotypic culture

568 - Single-cell RNA-sequencing analysis

569 - BIO and MeBIO treatment

570 QUANTIFICATION AND STATISTICAL ANALYSIS

571 - Image quantification

572 - Statistical analysis

573

574 **STAR ★ METHODS**

575 **KEY RESOURCES TABLE**

Reagent or resource	Source	Identifier
Primary antibodies		
Rat monoclonal anti-CD31	BD Biosciences	Cat #553370, RRID:AB_394816
FITC rat monoclonal anti-mouse CD31	BD Pharmingen	Cat #553372, RRID:AB_394818
APC rat monoclonal anti-mouse CD31	BD Pharmingen	Cat #551262, RRID:AB_398497
Rabbit monoclonal anti-Ki67	Abcam	Cat #ab16667, RRID:AB_302459
Rabbit monoclonal anti-Cleaved Caspase-3	Cell Signaling Technology	Cat #9664S, RRID:AB_2070042
Goat polyclonal anti-DLL4	R & D Systems	Cat #AF1389, RRID:AB_354770
Rabbit polyclonal anti-Claudin-5	ThermoFisher Scientific	Cat #34-1600, RRID:AB_2533157
Mouse monoclonal anti-ZO-1	ThermoFisher Scientific	Cat #33-9100, RRID:AB_2533147
Rabbit polyclonal anti-SOX9	Millipore Sigma	Cat #ABE571, Lot #2535307
Mouse monoclonal anti-Glutamine synthetase	Millipore Sigma	Cat #MAB302, RRID:AB_2110656

Rabbit monoclonal anti-EAAT1 (GLAST)	Abcam	Cat #ab181036, RRID:AB_2885103
Rabbit polyclonal anti-EAAT2 (GLT-1)	Abcam	Cat #ab41621, RRID:AB_941782
Rabbit polyclonal anti-GFAP	Millipore Sigma	Cat #AB5804, RRID:AB_2109645
Rat monoclonal anti-CD140a (PDGFRα)	BD Biosciences	Cat #558774, RRID:AB_397117
Rabbit monoclonal anti-LEF1	Cell Signaling Technology	Cat# 2230s, RRID:AB_823558
Goat polyclonal anti-PDGFRβ	R & D Systems	Cat #AF1042, RRID:AB_2162633
Rabbit polyclonal anti-Laminin	Millipore Sigma	Cat #L9393, RRID:AB_477163
Rabbit polyclonal anti-Collagen IV	Abcam	Cat #ab6586, RRID:AB_305584
Rabbit polyclonal anti-Aquaporin-4	Millipore Sigma	Cat #A5971, RRID:AB_258270
Rabbit polyclonal anti-Caveolin-1	Abcam	Cat #ab18199, RRID:AB_444314
Rabbit polyclonal anti-PLVAP	Proteintech	Cat #14452-1-AP, RRID:AB_2166100
Mouse monoclonal anti-NeuN	Millipore Sigma	Cat #MAB377, RRID:AB_2298772

Rabbit polyclonal anti-Calbindin	Millipore Sigma	Cat #AB1778, RRID:AB_2068336
Mouse monoclonal anti-PKCα	Santa Cruz Biotechnology	Cat #sc-8393, RRID:AB_628142
Goat polyclonal anti-Podocalyxin	R & D Systems	Cat #AF1556-SP, RRID:AB_354858
Goat polyclonal anti-Choline Acetyltransferase (ChAT)	Novus Biologicals	Cat #NBP1-30052, RRID:AB_1968484
Mouse monoclonal anti-GAD67	Millipore Sigma	Cat #MAB5406, RRID:AB_2278725
Rabbit polyclonal anti-Tyrosine Hydroxylase (TH)	Abcam	Cat #ab6211, RRID:AB_2240393
Rabbit polyclonal anti-Mfsd2a	Gift from Dr. Chenghua Gu (Cell Signaling Technology)	Cat #14-87 Mfsd2a, RRID:AB_2617168
Rabbit monoclonal anti-Hexokinase II	Abcam	Cat #ab209847, RRID:AB_2904621
Rabbit monoclonal anti-Pyruvate kinase M2	Cell Signaling Technology	Cat #4053, RRID:AB_1904096
Rabbit polyclonal anti-VEGF-A	Millipore Sigma	Cat #SAB5700629
Mouse monoclonal anti-GAPDH	Proteintech	Cat #60004-1-Ig, RRID:AB_2107436
Chemicals, peptides, and recombinant proteins		

Biocytin-TMR (5-(and-6)-tetramethylrhodamine biocytin)	ThermoFisher Scientific	Cat #T12921
Bovine Serum Albumin (BSA), AlexaFluor 594 conjugate	ThermoFisher Scientific	Cat #A13101
Fluorescein-labeled *Griffonia* (*Bandeiraea*) *Simplicifolia* Lectin I (GSL I, BSL I)	Vector Laboratories	Cat #FL-1101, RRID:AB_2336490
Rhodamine-labeled *Griffonia* (*Bandeiraea*) *Simplicifolia* Lectin I (GSL I, BSL I)	Vector Laboratories	Cat #RL-1102, RRID:AB_2336492
Hypoxyprobe™-1 Kit (100 mg of Pimonidazole HCl plus 1 ml of 11.23.22.r rat monoclonal antibody	Hypoxyprobe	Cat #HP1-100Kit
6-BIO ((2*Z*,3*E*)-6-bromoindirubin- 3-acetoxime, BIO-Acetoxime)	Calbiochem	Cat #361551
MeBIO (1-methyl-BIO)	Calbiochem	Cat #361556
Propidium iodide	ThermoFisher Scientific	Cat #P1304MP
TFB-TBOA	TOCRIS	Cat #2532
CD16/CD32 Fc block	BD Pharmingen	Cat #553141
Experimental Models: Organisms/Strains		
Vglut1$^{+/-}$ (C57/BL6J background)	Gift from Dr. Robert H. Edwards [71]	N/A

Gnat1$^{+/-}$ (C57/BL6J background)	Gift from Dr. William J. Brunken [26]	N/A
Chrnb2$^{+/-}$ (C57/BL6J background)	Gift from Dr. Marina Picciotto [11]	N/A
Oligonucleotides		
Vglut1-WT forward: 5'CCAAGCAAGGTTAAGCCTAG3'	IDT	N/A
Vglut1-WT reverse: 5'GGTGAATTTGGAAAAGAGC3'	IDT	N/A
Vglut1-KO forward: 5'TCGCAGCGCATCGCCTTCTA3'	IDT	N/A
Vglut1-KO reverse: 5'GCCACACGTTTCTTCTGAGG3'	IDT	N/A
Gnat1-WT forward: 5'GCCATCATCTACGGCAACACT CTGC3'	IDT	N/A
Gnat1-WT reverse: 5'GCCGGCGGAATTGAGCTGGTA 3'	IDT	N/A
Gnat1-KO forward: 5'GCCGGTGAATCCGGGAAGAGC 3'	IDT	N/A
Gnat1-KO reverse:	IDT	N/A

5'GGGCTGCTAAAGCGCATGCTC 3'		
Chrnb2-WT forward: *5'*CGGAGCATTTGAACTCTG AGCAGTGGGGTCGC3'	IDT	N/A
Chrnb2-WT reverse: 5'CTCGCTGACACAAGGGCT GCGGAC3'	IDT	N/A
Chrnb2-KO forward: *5'*CACTACGTCTGAACG TCGAAAACCCG3'	IDT	N/A
Chrnb2-KO reverse: 5'CGGGCAAATAATATC GGTGGCCGTGG3'	IDT	N/A
Softwares and algorithms		
ImageJ/Fiji	NIH	https://imagej.net/software/fiji/downloads
Zen microscopy software	ZEISS	https://www.zeiss.com/microscopy/en/products/software/zeiss-zen.html#packages
Seurat	Seurat	https://satijalab.org/seurat/
Tidyverse	Tidyverse	https://www.tidyverse.org

DAVID	DAVID bioinformatics resources	https://david.ncifcrf.gov
Prism 9	GraphPad	https://www.graphpad.com/scientific-software/prism/
Other		
RNA *in situ* probe for mouse *Ndp* (Norrin)	[36]	N/A
C57B6 wild-type P14 retina by drop-seq (single-cell RNA-sequencing database)	[48]	https://singlecell.broadinstitute.org/single_cell/study/SCP301/c57b6-wild-type-p14-retina-by-drop-seq

576

577 **RESOURCE AVAILABILITY**

578 **Lead contact**

579 Further information and requests for resources and reagents should be directed to the lead contact, Dritan
580 Agalliu (da191@cumc.columbia.edu).

581

582 **Materials availability**

583 This study did not generate new unique reagents.

584

585 **Data and code availability**

586 All data are available in the manuscript and the supplementary information. The codes used in this study
587 have been previously published and are freely available (see Key Resources Table). Any additional
588 information required to reanalyze the data reported in this study will be available upon request.

589

590 **EXPERIMENTAL MODEL AND SUBJECT DETAILS**

591 **Mice**

592 All animal usage and protocols were approved by the Institutional Animal Care and Use Committee
593 (IACUC) at Columbia University Irving Medical Center. Experimental procedures were optimized to
594 minimize animal stress and the number of animals used for experiments. Mice were maintained on 12
595 light/12 dark cycle. Both sexes (males and females) were used for experiments and analyses. All mice were
596 maintained in C57/BL6J background. The *in vivo* BRB permeability assays were performed either at P10
597 or P14. Generation of *Vglut1*$^{-/-}$ mice was described before [71]. These mice were bred as heterozygous and
598 gave birth in Mendelian ratios. Age-matched littermate WT and *Vglut1*$^{-/-}$ mice were used for experiments
599 (*Vglut1*$^{-/-}$ mice die around P15). Generation of *Gnat1*$^{-/-}$ mice was described before [26]. These mice were bred
600 as heterozygous and gave birth in Mendelian ratios. Age-matched littermate WT and *Gnat1*$^{-/-}$ mice were
601 used for experiments. *Gnat1*$^{-/-}$ mice are viable and fertile. Generation of *Chrnb2*$^{-/-}$ mice was described
602 before [11]. These mice were bred as *Chrnb2*$^{+/-}$ and gave birth in Mendelian ratios. Age-matched littermate
603 WT and *Chrnb2*$^{-/-}$ mice were used for experiments. *Chrnb2*$^{-/-}$ mice are viable and fertile.

604

605 **METHOD DETAILS**

606 **Immunofluorescence**

607 Unless otherwise specified, isolated tissues (retina, brain and liver) were fixed in 4% PFA for 2
608 hours for immunostaining. The exceptions were retinal flat-mount staining for Laminin, in which cases
609 retinas were fixed for 10 minutes in 2% PFA. For retinal flat-mounts, tissues were washed with 1X PBS
610 following PFA fixation and blocked overnight in blocking buffer (5% goat or donkey serum, 0.3% Triton
611 X-100 in 1× PBS) at 4°C. Samples were then incubated with primary antibodies in antibody-diluting
612 solution (5% goat or donkey serum; 0.01% Triton X-100 in 1X PBS) for 48h at 4°C, washed, and incubated
613 with secondary antibodies for 24 hours. For radial section staining, samples were washed in 1 × PBS,

614 cryoprotected in 30% sucrose overnight, embedded in optimal cutting temperature compound (OCT;
615 Tissue-Tek; Torrance, CA, USA), and sectioned at a thickness of 12 µm. Tissue sections were blocked for
616 2h at room temperature followed by primary antibody incubation overnight at 4°C. Following 1X PBS
617 washes, sections were incubated with secondary antibodies for 4h at room temperature. Samples were
618 imaged in room temperature using a Zeiss LSM700 confocal microscope [ZEISS 20X air (Objective Plan-
619 Apochromat 20x/0.8 M27; numerical aperture: 0.8) or 40X water (Objective C-Apochromat 40x/1.2 W
620 autocorr M27; numerical aperture: 1.2) objectives; ZEN image acquisition software] and analyzed using
621 Fiji software.
622
623 **Western blotting**
624 Retinas were collected from mice after perfusion with PBS. Six retinas from three mice were
625 combined for each sample. Collected tissue was homogenized in lysis buffer containing protease and
626 phosphatase inhibitors using a Dounce homogenizer followed by sonication. Protein concentration was
627 assayed by BCA (Bio-Rad) and resolved on SDS-PAGE. Protein levels in P10 retinas were measured by
628 fluorescent western blot analysis [4-15% or 7.5% Mini-PROTEAN TGX gels (Bio-Rad)] and quantitation
629 was performed using the LICOR system, as previously described. Fluorescent quantification of protein
630 levels was performed using the Odyssey SA infrared imaging system. Values are displayed as protein levels
631 corrected with GAPDH (loading control) and normalized to the WT values.
632
633 **Antibodies**
634 Primary antibodies used were rat anti-CD31 (BD Biosciences, Cat #553370, 1:250), rabbit anti-
635 Ki67 (Abcam, Cat #ab16667, 1:500), rabbit anti-cleaved Caspase-3 (Cell Signaling Technology, Cat
636 #9664S, 1:500), Goat anti-DLL4 (R & D Systems, Cat #AF1389, 1:200), rabbit anti-Claudin-5
637 (ThermoFisher Scientific, Cat #34-1600, 1:500), rabbit anti-SOX9 (Millipore Sigma, Cat #ABE571, 1:500),
638 mouse anti-Glutamine Synthetase (Millipore Sigma, Cat #MAB302, 1:500), rabbit anti-EAAT1 (Abcam,

639 Cat #ab181036, 1:250), rabbit anti-EAAT2 (Abcam, Cat #ab41621, 1:250), rabbit anti-GFAP (Millipore
640 Sigma, Cat #AB5804, 1:500), rat anti-CD140a (BD Biosciences, Cat #558774, 1:100), rabbit anti-LEF1
641 (Cell Signaling Technology, Cat #2230s, 1:100), goat anti-PDGFRβ (R & D Systems, Cat #AF1042, 1:250),
642 rabbit anti-Laminin (Millipore Sigma, Cat #L9393, 1:500), rabbit anti-Aquaporin-4 (Millipore Sigma, Cat
643 #A5971, 1:250), rabbit anti-Caveolin-1 (Abcam, Cat #ab18199, 1:500), rabbit anti-PLVAP (Proteintech,
644 Cat #14452-1-AP, 1:250), mouse anti-NeuN (Millipore Sigma, Cat #MAB377, 1:500), rabbit anti-
645 Calbindin (Millipore Sigma, Cat #AB1778, 1:250), mouse anti-PKCα (Santa Cruz Biotechnology, Cat #sc-
646 8393, 1:1000), rabbit anti-Mfsd2a (a gift from Dr. Chenghua Gu, 1:300), goat anti-Podocalyxin (R & D
647 Systems, Cat #AF1556-SP, 1:500), goat anti-ChAT (Novus Biologicals, Cat #NBP1-30052, 1:100), mouse
648 anti-GAD67 (Millipore Sigma, Cat #MAB5406, 1:2000), rabbit anti-Tyrosine Hydroxylase (Abcam, Cat
649 #ab6211, 1:1000), rabbit anti-Hexokinase II (Abcam, Cat #ab209847, 1:1000), rabbit anti-Pyruvate Kinase
650 M2 (Cell Signaling Technology, Cat #4053, 1:1000), rabbit anti-VEGF-A (Millipore Sigma, Cat
651 #SAB5700629, 1:2000), mouse anti-GAPDH (Proteintech, Cat #60004-1-Ig, 1:50000), FITC rat anti-
652 mouse CD31 (BD Pharmingen, Cat #553372, 1:200), and APC rat anti-mouse CD31 (BD Pharmingen, Cat
653 #551262, 1:200). Secondary antibodies used were: goat anti-rat Alexa Fluor 594 (A11007), goat anti-rabbit
654 Alexa Fluor 594 (A11012), goat anti-rat Alexa Fluor 488 (A11006), goat anti-rabbit Alexa Fluor 488
655 (A11034), donkey anti-rat Alexa Fluor 594 (A21209), donkey anti-rabbit Alexa Fluor 594 (A32754),
656 donkey anti-rat Alexa Fluor 488 (A21208), donkey anti-rabbit Alexa Fluor 488 (A21206), donkey anti-rat
657 Alexa Fluor 647 (A48272), donkey anti-rabbit Alexa Fluor 647 (A32795), donkey anti-goat Alexa Fluor
658 594 (A32758) and donkey anti-goat Alexa Fluor 488 (A11055) (all 1:250; ThermoFisher
659 Scientific). IRDyes 680 and 800 (1:20000; LI-COR) were used as secondary antibodies for Western blot.
660

661 ***In situ* hybridization**

662 Both alkaline phosphatase and fluorescent *in situ* hybridization of fresh-frozen (in OCT) retinal
663 sections using antisense mRNA probe for full-length mouse *Ndp* (Norrin) were performed as described

664 before [36]. The samples were imaged using either a ZEISS Axio Imager (alkaline phosphatase) or a ZEISS
665 LSM700 confocal (fluorescent) microscope and analyzed using Fiji software.
666
667 **Barrier permeability assays**
668 Mice were anesthetized using isoflurane and injected with either 1% Biocytin-5(and-6-)-
669 Tetramethylrhodamine (biocytin-TMR: ThermoFisher Scientific, Cat #T12921) or 1% Bovine Serum
670 Albumin (BSA) - AlexaFluor 594 conjugate (albumin-Alexa594: ThermoFisher Scientific, Cat #A13101)
671 into the tail veins. After 40 minutes in circulation, mice were re-anesthetized and perfused with 1X PBS via
672 the cardiac route. Retinas and livers were isolated and fixed in 4% PFA for 2 hours prior to immunostaining
673 with FITC-conjugated Lectin. Since blood vessels in the liver do not have a barrier, Biocytin-TMR or
674 Albumin-594 fluorescence levels in the livers of corresponding animals were used as internal controls for
675 measurement of biocytin-TMR and albumin-Alexa594 fluorescence levels in the retinas as described [36,37].
676
677 **Vessel perfusion assay**
678 P14 pups were anesthetized using isoflurane and injected with 75 µl of Rhodamine-labeled Lectin
679 (Vector Laboratories, Cat #RL-1102) into the left ventricles of the heart. Lectin was allowed to circulate
680 for 5 minutes under anesthesia. After that, retinas were isolated and fixed in 4% PFA for 2 hours prior to
681 immunostaining with vascular markers.
682
683 **Hypoxia measurement**
684 Hypoxyprobe staining was performed as per the vendor's (Hypoxyprobe, Cat #HP1-100Kit)
685 instructions. Briefly, the probe was dissolved in saline and administered into P10 pups by intraperitoneal
686 injection at a concentration of 60 mg/kg body weight. After 90 minutes, the pups were anesthetized using
687 isoflurane and perfused for 4 minutes with ice-cold sterile 1X PBS. After this, retinas were harvested,
688 washed with 1X PBS following PFA fixation (4% PFA for 2 hours) and blocked overnight in blocking

689 buffer at 4°C. Samples were then incubated with primary antibody (11.23.22.r) provided with the kit in
690 antibody-diluting solution (1:50) for 48h at 4°C. Retinas were then washed with 1X PBS, and incubated
691 with secondary donkey anti-rat Alexa594 antibody and Fluorescein-labeled Lectin for 24h.
692
693 **Retinal organotypic culture**
694 P10 WT pups were perfused with sterile 1X PBS under isoflurane-induced anesthesia, and eyeballs
695 were enucleated. Eyeballs were dissected in sterile neurobasal media (ThermoFisher Scientific, Cat
696 #21103049) supplemented with serum free B-27 (ThermoFisher Scientific, Cat #17504044). Corneas and
697 lenses were removed from the eyeballs, and eyecups were placed in the upper chambers of sterile 12 mm
698 Transwell with 0.4 μm Pore Polycarbonate Membrane Insert (Corning Life Sciences, Cat #3401). Eyecups
699 were divided into four groups based on the media (neurobasal media + B-27) composition: 1) without
700 glutamate, 2) with 0.1 mM glutamate, 3) without glutamate + 100 μm TFB-TBOA, 4) with 0.1 mM
701 glutamate + 100 μm TFB-TBOA. The upper chambers of the transwell received 350 μl of the corresponding
702 media, and the lower chambers of the transwell received 650 μl of the corresponding media. Under these
703 conditions, the eyecups were placed in the sterile incubator for either 6 hours or 12 hours at 37° C and with
704 5% CO_2. After 6 or 12 hours, the eyecups were removed from trans-well and fresh-frozen in OCT for future
705 sectioning and fluorescent *in situ* hybridization.
706
707 **Retinal endothelial cell isolation**
708 P10 WT and *Vglut1*$^{-/-}$ as well as P14 WT mice were anesthetized using isoflurane and perfused for
709 4 minutes with sterile 1X PBS. The eyes were enucleated and retinas were dissected in Earl's balanced salt
710 solution (EBSS). Retinas were dissociated in a single-cell suspension using a published protocol [80]. Once
711 the retinas were dissociated into single cells, it was resuspended in 200 ml of CD16/CD32 Fc block (BD
712 Pharmingen, Cat #553141, 1:200 in FACS buffer) and incubated at room temperature for 15 minutes. The
713 samples were washed with 2 ml of FACS buffer, with 100 ml kept aside for use as unstained and

714 fluorescence minus one (FMO) controls. The cells were then resuspended in 200 ml of anti-mouse CD31
715 [either FITC rat anti-mouse CD31 (BD Pharmingen, Cat #553372, 1:200) or and APC rat anti-mouse CD31
716 (BD Pharmingen, Cat #551262), 1:200 in FACS buffer)] antibody to label ECs, covered in aluminum foil
717 and incubated on ice for 60 mins. Following antibody labeling, the samples were washed twice with 2 ml
718 of FACS buffer and resuspended in 400 ml of propidium iodide (Thermofisher, Cat. #P1304MP; 1/10,000
719 in FACS buffer). Gates for the surface stain were set using the unstained and FMO controls, and either
720 CD31-APC^{+} or CD31-FITC^{+} ECs were sorted out using the BD FACSAria Flow Cytometer (Columbia
721 Stem Cell Initiative Flow Cytometry Core) for single-cell RNA-sequencing.
722
723 **Single-cell RNA-sequencing (scRNA-seq) analysis**
724 Total of 1104 ECs for P10 WT retinas and 1046 ECs for P10 *Vglut1*$^{-/-}$ retinas were analyzed for
725 differential gene expression analyses (**Table S1**). The 10x Genomics Chromium platform [81,82] was used to
726 generate low-depth data (~2000 genes/cell), and was processed using the Cell Ranger analysis pipeline to
727 align reads and generate feature-barcode matrices. The Seurat R package [83] was implemented to read the
728 output of the Cell Ranger pipeline and merge cells from all the samples (WT and mutant) into a single R
729 object. The standard pre-processing workflow for scRNAseq data was carried out in Seurat, which consisted
730 of the selection and filtration of cells based on quality control metrics (e.g., number of unique genes detected
731 in each cell > 200, total number of molecules detected within a cell > 1,000 and < 50,000, percentage of
732 reads within a cell that map to the mitochondrial genome < 20, etc.), data normalization and scaling, and
733 the detection of highly variable features. Next, linear dimensionality reduction (PCA) was performed on
734 the scaled data using the previously determined highly variable features, an alternative heuristic method
735 ('Elbow plot') was implemented to determine the 'dimensionality' of the dataset, and cells were clustered by
736 applying the weighted shared nearest-neighbor graph-based clustering method using the first 20 PCs [84].
737 Lastly, the 20 PCA dimensions were further reduced into two-dimensional space using the non-linear
738 dimensional reduction technique, uniform manifold approximation and projection for dimension reduction

739 (UMAP), to visualize and explore the scRNA-seq dataset and each of its unique EC clusters. All the ECs
740 isolated from either genotype were plotted in the UMAP. Differential gene expression analyses were
741 performed for all ECs from either genotype, and not on specific clusters. From the gene signatures that are
742 uniquely present in mutant ECs compared to WT ECs, and validated by fluorescent in situ hybridization
743 and/or immunofluorescence. Gene ontology (GO) enrichment analysis was performed using DAVID
744 bioinformatics database to elucidate significantly up- and downregulated pathways in mutant ECs.
745

746 **BIO and MeBIO treatment**

747 The *in vivo* injections of 6-BIO ((2*Z*,3*E*)-6-bromoindirubin- 3-acetoxime, BIO-Acetoxime;
748 Calbiochem, Cat #361551) and control MeBIO (1-methyl-BIO; Calbiochem, Cat #361556) were performed
749 as previously published [64]. Pups were anesthetized with 1% isoflurane. Intraperitoneal injections of BIO
750 and MeBIO were performed at a concentration of 5 mg/kg/day in sterile PBS from P6 to P8. Injected pups
751 were re-anesthetized and perfused with 1X PBS to harvest tissues for analyses at P10.
752

753 **QUANTIFICATION AND STATISTICAL ANALYSIS**

754 **Image quantification**

755 For retinal flat-mounts, each measurement was made in at least 3 quadrants per sample. The
756 measurements were done separately in the central (near the optic nerve-head) and peripheral (near the edge)
757 retina. For sections, at least three sections were imaged per sample. In each case, multiple representative
758 images were acquired and averaged. To measure vascular area and branch point density, area positive for
759 CD31 or Lectin was measured from each image in Fiji software (National Institutes of Health) using signal
760 masking. Branch point numbers were normalized to unit area (1 mm^2). To measure number of proliferative
761 or apoptotic ECs, the number of $Ki67^+$ or cleaved Caspase-3^+ ECs, respectively, were normalized to unit
762 $CD31^+$ vascular area (1 mm^2). The area of Biocytin-TMR leakage was done separately in the central and
763 peripheral retina. The intensity of biocytin-TMR and albumin-Alexa594 outside of retinal vessels was

764 measured as described [36]. Biocytin-TMR and albumin-Alexa594 signal intensities in the retina and cerebella
765 were normalized to those of livers. For vascular area positive for Claudin-5 and Caveolin-1, area positive
766 for Lectin was selected from each image in Fiji software using signal masking, followed by measuring the
767 percentage of Lectin$^+$/Claudin-5$^+$ or Lectin$^+$/Caveolin-1$^+$ in corresponding images. To measure the number
768 of ganglion (NeuN$^+$), amacrine, horizontal (Calbindin$^+$) and bipolar cells (PKCα^+), the number of cells were
769 normalized to the length of either ganglion cell layer (GCL; for ganglion cells) or inner nuclear layer (INL;
770 for amacrine, horizontal and bipolar cells). To measure the number of photoreceptors, the thickness of the
771 outer nuclear layer (ONL) was quantified as a function of photoreceptor number. To measure the number
772 of Müller glia, the number of Sox9$^+$ cells were normalized to the length of INL. To measure the relative
773 expression of GS and GLAST, the M.F.I were calculated for each field and data was presented as values
774 normalized to the number of Sox9$^+$ Müller glia. To measure *Ndp* expression, mean fluorescence intensity
775 (M.F.I) of *Ndp* in the INL was calculated with histogram analysis in Fiji software and normalized to the
776 WT values. For Lef1$^+$ EC quantification, the number of Lef1$^+$ ECs was normalized to unit CD31$^+$ or Lectin$^+$
777 vascular area (1 mm^2). For western blots, values are displayed as target protein levels corrected with
778 GAPDH (loading control) and normalized to the WT values using Odyssey SA infrared imaging system.
779

780 **Statistical analysis**

781 Retinas from 3-5 different animals (for *in vivo* experiments) were used for statistical analysis. For
782 western blots, retinas from 3 animals/genotype were combined into one sample, and 4 samples/genotype
783 was used for quantification. To test for statistical significance of any differences, unpaired Student's *t* test
784 or one-way ANOVA was performed using GraphPad Prism. A value of $P < 0.05$ was considered
785 statistically significant. For scRNA-seq analysis, we considered transcripts with adjusted p value < 0.05,
786 and >1.2-fold ($\log_2$fc > 0.25 and $\log_2$fc < -0.25) difference in expression as significant. For GO analysis,
787 Gene sets with false discovery rate (FDR) < 0.01 were considered significant.

788 **REFERENCES**

789 1 Klaassen, I., Van Noorden, C. J. & Schlingemann, R. O. Molecular basis of the inner blood-retinal
790 barrier and its breakdown in diabetic macular edema and other pathological conditions. *Prog Retin*
791 *Eye Res* **34**, 19-48, doi:10.1016/j.preteyeres.2013.02.001 (2013).
792 2 Zhao, Z., Nelson, A. R., Betsholtz, C. & Zlokovic, B. V. Establishment and Dysfunction of the
793 Blood-Brain Barrier. *Cell* **163**, 1064-1078, doi:10.1016/j.cell.2015.10.067 (2015).
794 3 Chow, B. W. & Gu, C. The molecular constituents of the blood-brain barrier. *Trends Neurosci* **38**,
795 598-608, doi:10.1016/j.tins.2015.08.003 (2015).
796 4 Biswas, S., Cottarelli, A. & Agalliu, D. Neuronal and glial regulation of CNS angiogenesis and
797 barriergenesis. *Development* **147**, doi:10.1242/dev.182279 (2020).
798 5 Umino, Y. & Solessio, E. Loss of scotopic contrast sensitivity in the optomotor response of diabetic
799 mice. *Invest Ophthalmol Vis Sci* **54**, 1536-1543, doi:10.1167/iovs.12-10825 (2013).
800 6 Pardue, M. T. *et al.* Rodent Hyperglycemia-Induced Inner Retinal Deficits are Mirrored in Human
801 Diabetes. *Transl Vis Sci Technol* **3**, 6, doi:10.1167/tvst.3.3.6 (2014).
802 7 Abcouwer, S. F. & Gardner, T. W. Diabetic retinopathy: loss of neuroretinal adaptation to the
803 diabetic metabolic environment. *Ann N Y Acad Sci* **1311**, 174-190, doi:10.1111/nyas.12412 (2014).
804 8 Feit-Leichman, R. A. *et al.* Vascular damage in a mouse model of diabetic retinopathy: relation to
805 neuronal and glial changes. *Invest Ophthalmol Vis Sci* **46**, 4281-4287, doi:10.1167/iovs.04-1361
806 (2005).
807 9 Feller, M. B., Wellis, D. P., Stellwagen, D., Werblin, F. S. & Shatz, C. J. Requirement for
808 cholinergic synaptic transmission in the propagation of spontaneous retinal waves. *Science* **272**,
809 1182-1187, doi:10.1126/science.272.5265.1182 (1996).
810 10 Zhou, Z. J. Direct participation of starburst amacrine cells in spontaneous rhythmic activities in the
811 developing mammalian retina. *J Neurosci* **18**, 4155-4165, doi:10.1523/JNEUROSCI.18-11-
812 04155.1998 (1998).
813 11 Bansal, A. *et al.* Mice lacking specific nicotinic acetylcholine receptor subunits exhibit dramatically
814 altered spontaneous activity patterns and reveal a limited role for retinal waves in forming ON and
815 OFF circuits in the inner retina. *J Neurosci* **20**, 7672-7681, doi:10.1523/JNEUROSCI.20-20-
816 07672.2000 (2000).
817 12 Blankenship, A. G. *et al.* Synaptic and extrasynaptic factors governing glutamatergic retinal waves.
818 *Neuron* **62**, 230-241, doi:10.1016/j.neuron.2009.03.015 (2009).
819 13 Tiriac, A., Smith, B. E. & Feller, M. B. Light Prior to Eye Opening Promotes Retinal Waves and
820 Eye-Specific Segregation. *Neuron* **100**, 1059-1065 e1054, doi:10.1016/j.neuron.2018.10.011
821 (2018).
822 14 Weiner, G. A. *et al.* Cholinergic neural activity directs retinal layer-specific angiogenesis and blood
823 retinal barrier formation. *Nat Commun* **10**, 2477, doi:10.1038/s41467-019-10219-8 (2019).
824 15 Bonezzi, P. J., Stabio, M. E. & Renna, J. M. The Development of Mid-Wavelength
825 Photoresponsivity in the Mouse Retina. *Curr Eye Res* **43**, 666-673,
826 doi:10.1080/02713683.2018.1433859 (2018).
827 16 Stahl, A. *et al.* The mouse retina as an angiogenesis model. *Invest Ophthalmol Vis Sci* **51**, 2813-
828 2826, doi:10.1167/iovs.10-5176 (2010).
829 17 Rao, S. *et al.* A direct and melanopsin-dependent fetal light response regulates mouse eye
830 development. *Nature* **494**, 243-246, doi:10.1038/nature11823 (2013).
831 18 Nguyen, M. T. *et al.* An opsin 5-dopamine pathway mediates light-dependent vascular development
832 in the eye. *Nat Cell Biol* **21**, 420-429, doi:10.1038/s41556-019-0301-x (2019).
833 19 Luhmann, U. F. *et al.* Role of the Norrie disease pseudoglioma gene in sprouting angiogenesis
834 during development of the retinal vasculature. *Invest Ophthalmol Vis Sci* **46**, 3372-3382,
835 doi:10.1167/iovs.05-0174 (2005).

836 20 Ye, X. *et al.* Norrin, frizzled-4, and Lrp5 signaling in endothelial cells controls a genetic program
837 for retinal vascularization. *Cell* **139**, 285-298, doi:10.1016/j.cell.2009.07.047 (2009).
838 21 Junge, H. J. *et al.* TSPAN12 regulates retinal vascular development by promoting Norrin- but not
839 Wnt-induced FZD4/beta-catenin signaling. *Cell* **139**, 299-311, doi:10.1016/j.cell.2009.07.048
840 (2009).
841 22 Xia, C. H., Yablonka-Reuveni, Z. & Gong, X. LRP5 is required for vascular development in deeper
842 layers of the retina. *PLoS One* **5**, e11676, doi:10.1371/journal.pone.0011676 (2010).
843 23 Zuercher, J., Fritzsche, M., Feil, S., Mohn, L. & Berger, W. Norrin stimulates cell proliferation in
844 the superficial retinal vascular plexus and is pivotal for the recruitment of mural cells. *Hum Mol*
845 *Genet* **21**, 2619-2630, doi:10.1093/hmg/dds087 (2012).
846 24 Paes, K. T. *et al.* Frizzled 4 is required for retinal angiogenesis and maintenance of the blood-retina
847 barrier. *Invest Ophthalmol Vis Sci* **52**, 6452-6461, doi:10.1167/iovs.10-7146 (2011).
848 25 Wang, Y. *et al.* Norrin/Frizzled4 signaling in retinal vascular development and blood brain barrier
849 plasticity. *Cell* **151**, 1332-1344, doi:10.1016/j.cell.2012.10.042 (2012).
850 26 Calvert, P. D. *et al.* Phototransduction in transgenic mice after targeted deletion of the rod transducin
851 alpha -subunit. *Proc Natl Acad Sci U S A* **97**, 13913-13918, doi:10.1073/pnas.250478897 (2000).
852 27 Schroeder, M. M. *et al.* The Roles of Rods, Cones, and Melanopsin in Photoresponses of M4
853 Intrinsically Photosensitive Retinal Ganglion Cells (ipRGCs) and Optokinetic Visual Behavior.
854 *Front Cell Neurosci* **12**, 203, doi:10.3389/fncel.2018.00203 (2018).
855 28 Okawa, H., Sampath, A. P., Laughlin, S. B. & Fain, G. L. ATP consumption by mammalian rod
856 photoreceptors in darkness and in light. *Curr Biol* **18**, 1917-1921, doi:10.1016/j.cub.2008.10.029
857 (2008).
858 29 Sherry, D. M., Wang, M. M., Bates, J. & Frishman, L. J. Expression of vesicular glutamate
859 transporter 1 in the mouse retina reveals temporal ordering in development of rod vs. cone and ON
860 vs. OFF circuits. *J Comp Neurol* **465**, 480-498, doi:10.1002/cne.10838 (2003).
861 30 Zarkada, G. *et al.* Specialized endothelial tip cells guide neuroretina vascularization and blood-
862 retina-barrier formation. *Dev Cell* **56**, 2237-2251 e2236, doi:10.1016/j.devcel.2021.06.021 (2021).
863 31 Siemerink, M. J., Klaassen, I., Van Noorden, C. J. & Schlingemann, R. O. Endothelial tip cells in
864 ocular angiogenesis: potential target for anti-angiogenesis therapy. *J Histochem Cytochem* **61**, 101-
865 115, doi:10.1369/0022155412467635 (2013).
866 32 Hellstrom, M. *et al.* Dll4 signalling through Notch1 regulates formation of tip cells during
867 angiogenesis. *Nature* **445**, 776-780, doi:10.1038/nature05571 (2007).
868 33 Suchting, S. *et al.* The Notch ligand Delta-like 4 negatively regulates endothelial tip cell formation
869 and vessel branching. *Proc Natl Acad Sci U S A* **104**, 3225-3230, doi:10.1073/pnas.0611177104
870 (2007).
871 34 Pelton, J. C., Wright, C. E., Leitges, M. & Bautch, V. L. Multiple endothelial cells constitute the tip
872 of developing blood vessels and polarize to promote lumen formation. *Development* **141**, 4121-
873 4126, doi:10.1242/dev.110296 (2014).
874 35 Chow, B. W. & Gu, C. Gradual Suppression of Transcytosis Governs Functional Blood-Retinal
875 Barrier Formation. *Neuron* **93**, 1325-1333 e1323, doi:10.1016/j.neuron.2017.02.043 (2017).
876 36 Mazzoni, J. *et al.* The Wnt Inhibitor Apcdd1 Coordinates Vascular Remodeling and Barrier
877 Maturation of Retinal Blood Vessels. *Neuron* **96**, 1055-1069 e1056,
878 doi:10.1016/j.neuron.2017.10.025 (2017).
879 37 Biswas, S. *et al.* Mural Wnt/beta-catenin signaling regulates Lama2 expression to promote
880 neurovascular unit maturation. *Development* **149**, doi:10.1242/dev.200610 (2022).
881 38 Bosma, E. K., van Noorden, C. J. F., Schlingemann, R. O. & Klaassen, I. The role of plasmalemma
882 vesicle-associated protein in pathological breakdown of blood-brain and blood-retinal barriers:
883 potential novel therapeutic target for cerebral edema and diabetic macular edema. *Fluids Barriers*
884 *CNS* **15**, 24, doi:10.1186/s12987-018-0109-2 (2018).

39 Gu, X. *et al.* Spatial and temporal localization of caveolin-1 protein in the developing retina. *Adv Exp Med Biol* **801**, 15-21, doi:10.1007/978-1-4614-3209-8_3 (2014).
40 Gu, X. *et al.* Loss of caveolin-1 causes blood-retinal barrier breakdown, venous enlargement, and mural cell alteration. *Am J Pathol* **184**, 541-555, doi:10.1016/j.ajpath.2013.10.022 (2014).
41 Buckingham, B. P. *et al.* Progressive ganglion cell degeneration precedes neuronal loss in a mouse model of glaucoma. *J Neurosci* **28**, 2735-2744, doi:10.1523/JNEUROSCI.4443-07.2008 (2008).
42 Hajdu, R. I. *et al.* Detailed Evaluation of Possible Ganglion Cell Loss in the Retina of Zucker Diabetic Fatty (ZDF) Rats. *Sci Rep* **9**, 10463, doi:10.1038/s41598-019-46879-1 (2019).
43 Usui, Y. *et al.* Neurovascular crosstalk between interneurons and capillaries is required for vision. *J Clin Invest* **125**, 2335-2346, doi:10.1172/JCI80297 (2015).
44 Poche, R. A., Furuta, Y., Chaboissier, M. C., Schedl, A. & Behringer, R. R. Sox9 is expressed in mouse multipotent retinal progenitor cells and functions in Muller glial cell development. *J Comp Neurol* **510**, 237-250, doi:10.1002/cne.21746 (2008).
45 Serjanov, D., Bachay, G., Hunter, D. D. & Brunken, W. J. Laminin beta2 Chain Regulates Retinal Progenitor Cell Mitotic Spindle Orientation via Dystroglycan. *J Neurosci* **38**, 5996-6010, doi:10.1523/JNEUROSCI.0551-18.2018 (2018).
46 Hippert, C. *et al.* Muller glia activation in response to inherited retinal degeneration is highly varied and disease-specific. *PLoS One* **10**, e0120415, doi:10.1371/journal.pone.0120415 (2015).
47 Lee, S. H., Park, Y. S., Paik, S. S. & Kim, I. B. Differential Response of Muller Cells and Microglia in a Mouse Retinal Detachment Model and Its Implications in Detached and Non-Detached Regions. *Cells* **10**, doi:10.3390/cells10081972 (2021).
48 Macosko, E. Z. *et al.* Highly Parallel Genome-wide Expression Profiling of Individual Cells Using Nanoliter Droplets. *Cell* **161**, 1202-1214, doi:10.1016/j.cell.2015.05.002 (2015).
49 Taylor, S., Srinivasan, B., Wordinger, R. J. & Roque, R. S. Glutamate stimulates neurotrophin expression in cultured Muller cells. *Brain Res Mol Brain Res* **111**, 189-197, doi:10.1016/s0169-328x(03)00030-5 (2003).
50 Shen, F. *et al.* Glutamate-induced glutamine synthetase expression in retinal Muller cells after short-term ocular hypertension in the rat. *Invest Ophthalmol Vis Sci* **45**, 3107-3112, doi:10.1167/iovs.03-0948 (2004).
51 Harada, T. *et al.* Functions of the two glutamate transporters GLAST and GLT-1 in the retina. *Proc Natl Acad Sci U S A* **95**, 4663-4666, doi:10.1073/pnas.95.8.4663 (1998).
52 Russo, R. *et al.* Impairment of neuronal glutamate uptake and modulation of the glutamate transporter GLT-1 induced by retinal ischemia. *PLoS One* **8**, e69250, doi:10.1371/journal.pone.0069250 (2013).
53 Cheng, S. Y. *et al.* Altered photoreceptor metabolism in mouse causes late stage age-related macular degeneration-like pathologies. *Proc Natl Acad Sci U S A* **117**, 13094-13104, doi:10.1073/pnas.2000339117 (2020).
54 Mackenzie, F. & Ruhrberg, C. Diverse roles for VEGF-A in the nervous system. *Development* **139**, 1371-1380, doi:10.1242/dev.072348 (2012).
55 Okabe, K. *et al.* Neurons limit angiogenesis by titrating VEGF in retina. *Cell* **159**, 584-596, doi:10.1016/j.cell.2014.09.025 (2014).
56 Schweighofer, B. *et al.* The VEGF-induced transcriptional response comprises gene clusters at the crossroad of angiogenesis and inflammation. *Thromb Haemost* **102**, 544-554, doi:10.1160/TH08-12-0830 (2009).
57 Liu, Y., Cox, S. R., Morita, T. & Kourembanas, S. Hypoxia regulates vascular endothelial growth factor gene expression in endothelial cells. Identification of a 5' enhancer. *Circ Res* **77**, 638-643, doi:10.1161/01.res.77.3.638 (1995).
58 Lee, M., Leskova, W., Eshaq, R. S. & Harris, N. R. Retinal hypoxia and angiogenesis with methamphetamine. *Exp Eye Res* **206**, 108540, doi:10.1016/j.exer.2021.108540 (2021).

934 59 Morita, A. *et al.* Transient phenotypic changes in endothelial cells and pericytes in neonatal mouse
935 retina following short-term blockade of vascular endothelial growth factor receptors. *Dev Dyn* **247**,
936 699-711, doi:10.1002/dvdy.24614 (2018).
937 60 Hupe, M. *et al.* Gene expression profiles of brain endothelial cells during embryonic development
938 at bulk and single-cell levels. *Sci Signal* **10**, doi:10.1126/scisignal.aag2476 (2017).
939 61 Jiang, E., Yan, X. & Weng, H. R. Glial glutamate transporter and glutamine synthetase regulate
940 GABAergic synaptic strength in the spinal dorsal horn. *J Neurochem* **121**, 526-536,
941 doi:10.1111/j.1471-4159.2012.07694.x (2012).
942 62 Sullivan, S. J. & Miller, R. F. AMPA receptor mediated D-serine release from retinal glial cells. *J*
943 *Neurochem* **115**, 1681-1689, doi:10.1111/j.1471-4159.2010.07077.x (2010).
944 63 Shimamoto, K. *et al.* Characterization of novel L-threo-beta-benzyloxyaspartate derivatives, potent
945 blockers of the glutamate transporters. *Mol Pharmacol* **65**, 1008-1015, doi:10.1124/mol.65.4.1008
946 (2004).
947 64 Corada, M. *et al.* Fine-Tuning of Sox17 and Canonical Wnt Coordinates the Permeability Properties
948 of the Blood-Brain Barrier. *Circ Res* **124**, 511-525, doi:10.1161/CIRCRESAHA.118.313316
949 (2019).
950 65 Carmeliet, P. & Tessier-Lavigne, M. Common mechanisms of nerve and blood vessel wiring.
951 *Nature* **436**, 193-200, doi:10.1038/nature03875 (2005).
952 66 Sapieha, P. Eyeing central neurons in vascular growth and reparative angiogenesis. *Blood* **120**,
953 2182-2194, doi:10.1182/blood-2012-04-396846 (2012).
954 67 Joyal, J. S. *et al.* Retinal lipid and glucose metabolism dictates angiogenesis through the lipid sensor
955 Ffar1. *Nat Med* **22**, 439-445, doi:10.1038/nm.4059 (2016).
956 68 Sapieha, P. *et al.* The succinate receptor GPR91 in neurons has a major role in retinal angiogenesis.
957 *Nat Med* **14**, 1067-1076, doi:10.1038/nm.1873 (2008).
958 69 Liang, J. H. *et al.* Dopamine signaling from ganglion cells directs layer-specific angiogenesis in the
959 retina. *Curr Biol* **33**, 3821-3834 e3825, doi:10.1016/j.cub.2023.07.040 (2023).
960 70 Boccuni, I. & Fairless, R. Retinal Glutamate Neurotransmission: From Physiology to
961 Pathophysiological Mechanisms of Retinal Ganglion Cell Degeneration. *Life (Basel)* **12**,
962 doi:10.3390/life12050638 (2022).
963 71 Fremeau, R. T., Jr. *et al.* Vesicular glutamate transporters 1 and 2 target to functionally distinct
964 synaptic release sites. *Science* **304**, 1815-1819, doi:10.1126/science.1097468 (2004).
965 72 Boye, K. *et al.* Endothelial Unc5B controls blood-brain barrier integrity. *Nat Commun* **13**, 1169,
966 doi:10.1038/s41467-022-28785-9 (2022).
967 73 Jones, B. W. *et al.* Retinal remodeling in human retinitis pigmentosa. *Exp Eye Res* **150**, 149-165,
968 doi:10.1016/j.exer.2016.03.018 (2016).
969 74 Jones, B. W. *et al.* Retinal Remodeling and Metabolic Alterations in Human AMD. *Front Cell*
970 *Neurosci* **10**, 103, doi:10.3389/fncel.2016.00103 (2016).
971 75 Pfeiffer, R. L., Marc, R. E., Kondo, M., Terasaki, H. & Jones, B. W. Muller cell metabolic chaos
972 during retinal degeneration. *Exp Eye Res* **150**, 62-70, doi:10.1016/j.exer.2016.04.022 (2016).
973 76 Chan-Ling, T. & Stone, J. Degeneration of astrocytes in feline retinopathy of prematurity causes
974 failure of the blood-retinal barrier. *Invest Ophthalmol Vis Sci* **33**, 2148-2159 (1992).
975 77 Prokofyeva, E. & Zrenner, E. Epidemiology of major eye diseases leading to blindness in Europe:
976 a literature review. *Ophthalmic Res* **47**, 171-188, doi:10.1159/000329603 (2012).
977 78 Liegl, R., Hellstrom, A. & Smith, L. E. Retinopathy of prematurity: the need for prevention. *Eye*
978 *Brain* **8**, 91-102, doi:10.2147/EB.S99038 (2016).
979 79 Lacoste, B. *et al.* Sensory-related neural activity regulates the structure of vascular networks in the
980 cerebral cortex. *Neuron* **83**, 1117-1130, doi:10.1016/j.neuron.2014.07.034 (2014).
981 80 Vanlandewijck, M. *et al.* A molecular atlas of cell types and zonation in the brain vasculature.
982 *Nature* **554**, 475-480, doi:10.1038/nature25739 (2018).

983 81 Yuan, J. & Sims, P. A. An Automated Microwell Platform for Large-Scale Single Cell RNA-Seq.
984 *Sci Rep* **6**, 33883, doi:10.1038/srep33883 (2016).
985 82 Yuan, J. *et al.* Single-cell transcriptome analysis of lineage diversity in high-grade glioma. *Genome*
986 *Med* **10**, 57, doi:10.1186/s13073-018-0567-9 (2018).
987 83 Hao, Y. *et al.* Integrated analysis of multimodal single-cell data. *Cell* **184**, 3573-3587 e3529,
988 doi:10.1016/j.cell.2021.04.048 (2021).
989 84 Menon, V. Clustering single cells: a review of approaches on high-and low-depth single-cell RNA-
990 seq data. *Brief Funct Genomics* **17**, 240-245, doi:10.1093/bfgp/elx044 (2018).
991

992 **FIGURES AND FIGURE LEGENDS**

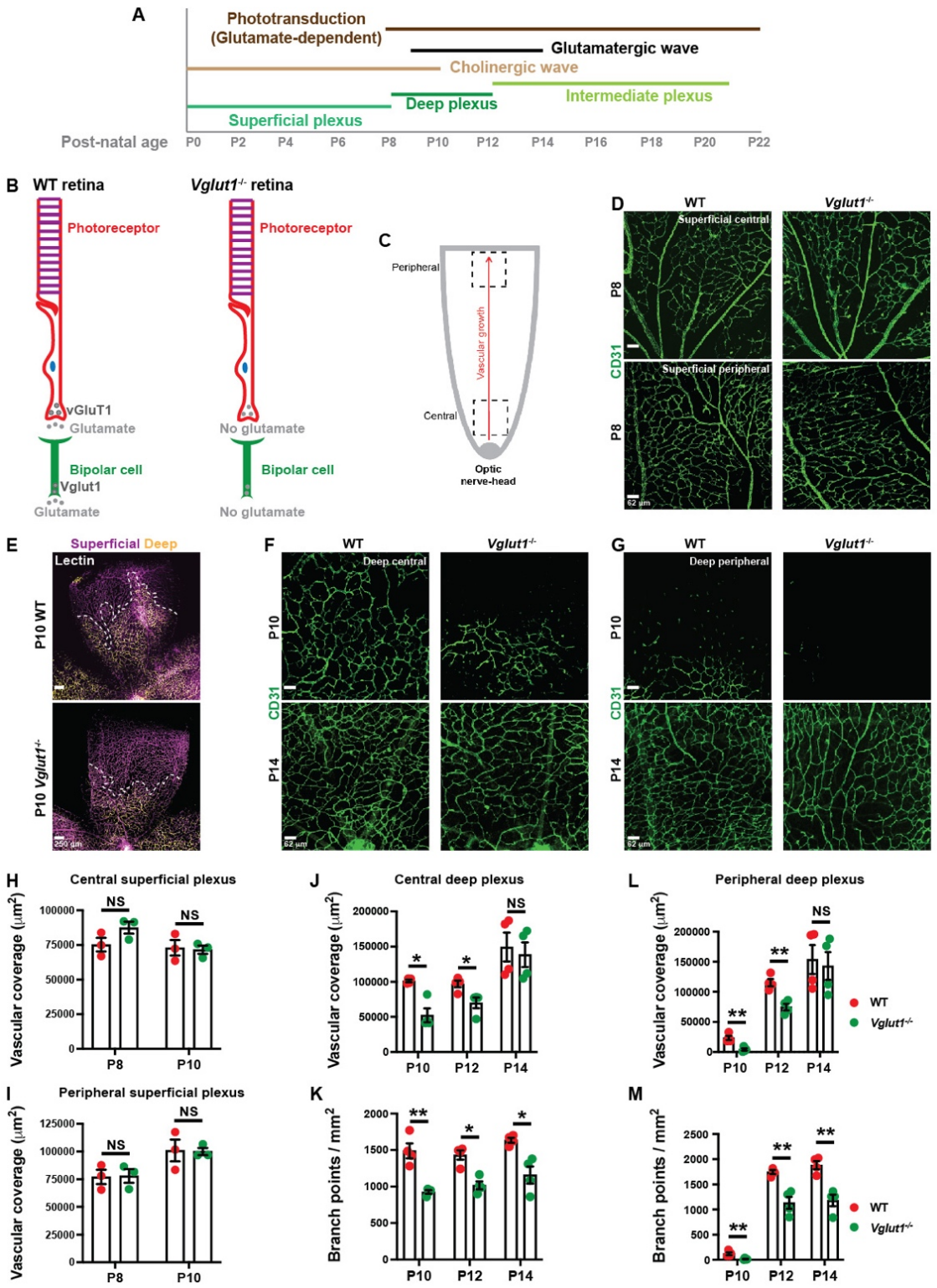

993

994

995 **Figure 1. Deep plexus angiogenesis is delayed in the *Vglut1*$^{-/-}$ retina. A)** Timeline of the neuronal activity

996 [cholinergic and glutamatergic waves and glutamatergic synaptic activity of photoreceptors

997 (phototransduction)] and angiogenesis (superficial, deep and intermediate plexuses) in the postnatal wild-
998 type (WT) retina (P1-P22). **B)** Schematic diagram of glutamate release from bipolar cells and
999 photoreceptors in WT and *Vglut1*$^{-/-}$ retinas. *Vglut1*$^{-/-}$ photoreceptors and bipolar cells fail to release
.000 glutamate into the synaptic cleft. **C)** Schematic diagram of distinct developmental regions in the retina.
.001 Central retina is developmentally more mature than peripheral retina. **D)** Representative images of the
.002 superficial plexus from P8 WT and *Vglut1*$^{-/-}$ retinal flat mounts stained for CD31 (green; EC marker). **E)**
.003 Representative images of the retinas from P10 WT and *Vglut1*$^{-/-}$ retinal flat mounts stained for CD31.
.004 Superficial plexus is color-coded in purple and deep plexus is color-coded in yellow. Dashed white line
.005 shows the extent of deep plexus vascularization. **F, G)** Representative images of the deep plexus from P10
.006 and P14 WT and *Vglut1*$^{-/-}$ retinal flat mounts visualized with CD31 staining (green). **H, I)** Dotted bar graphs
.007 of the vascular coverage of the superficial plexus in P8 and P10 WT and *Vglut1*$^{-/-}$ central (**H**) and peripheral
.008 (**I**) retina (n = 3 mice/genotype). **J-M)** Dotted bar graphs of the vascular coverage (**J, L**) and branch point
.009 density (**K, M**) of the deep plexus in P10, P12 and P14 WT and *Vglut1*$^{-/-}$ central (**J, K**) and peripheral (**L,**
.010 **M**) retina (n = 4 mice/genotype). Scale bars: E = 250 μm; D, F, G = 62 μm. Statistical analyses were done
.011 with Students t-test: *$p<0.05$, **$p<0.02$, NS = not significant. Error bars: Mean ± S.E.M.
.012

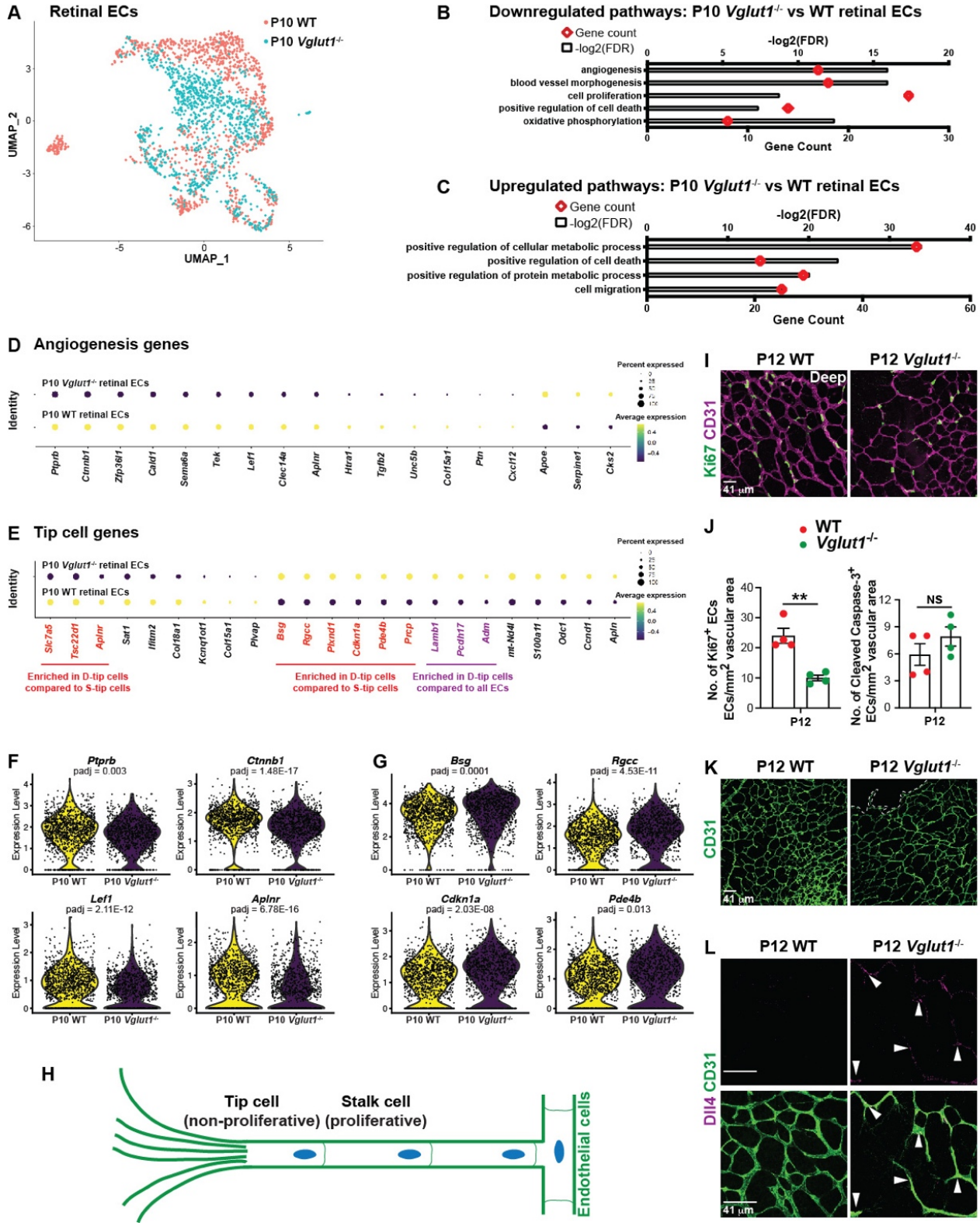

Figure 2. Aberrant angiogenic transcriptomic signatures are present in *Vglut1*$^{-/-}$ ECs from single cell RNA-sequencing (scRNA-seq). A) A Uniform Manifold Approximation and Projection (UMAP) for

.017 dimension reduction projection shows separation of P10 WT and *Vglut1*$^{-/-}$ retinal ECs based on their
.018 transcriptomic signatures. **B, C)** Gene ontology (GO) analyses of P10 WT and *Vglut1*$^{-/-}$ retinal ECs show
.019 top downregulated (**B**) and upregulated (**C**) pathways. **D, E)** Dot plot of expression levels for angiogenesis
.020 (**D**) and tip cell (**E**) genes in P10 WT and *Vglut1*$^{-/-}$ retinal ECs. The dot size indicates the percent of the
.021 population expressing each marker, the color scale indicates the average level of gene expression. Genes
.022 enriched in deep plexus tip cells (D-tip cells) compared to superficial plexus tip cells (S-tip cells) are shown
.023 in red. Genes enriched in deep plexus tip cells (D-tip cells) compared to all ECs are shown in purple. **F, G)**
.024 Violin plots of representative angiogenesis (**F**) and tip cells (**G**) genes in P10 WT and *Vglut1*$^{-/-}$ retinal ECs.
.025 **H)** Schematic of a vascular sprout consisting of leading tip cells and proliferative stalk cells. **I)**
.026 Representative images of the deep plexus from P12 WT and *Vglut1*$^{-/-}$ retinal flat-mounts stained for Ki67
.027 (green) and CD31 (purple). **J)** Measurements of Ki67^{+} (proliferative), or cleaved Caspase3^{+} (apoptotic) ECs
.028 in P12 WT and *Vglut1*$^{-/-}$ retinal deep plexus (n = 4). **K)** Representative images of the deep plexus from P12
.029 WT and *Vglut1*$^{-/-}$ retinal flat-mounts stained for CD31 (green). The dotted line shows the border of the
.030 vascular front in the *Vglut1*$^{-/-}$ retina. **L)** Representative images of the deep plexus from P12 WT and *Vglut1*$^{-}$
.031 $^{/-}$ retinal flat-mounts stained for CD31 and Dll4. Arrowheads point to Dll4^{+} tip cells in the *Vglut1*$^{-/-}$ retina.
.032 Scale bars = 41 μm. Students t-test: **<0.02, NS = not significant. Error bars: Mean ± S.E.M.
.033

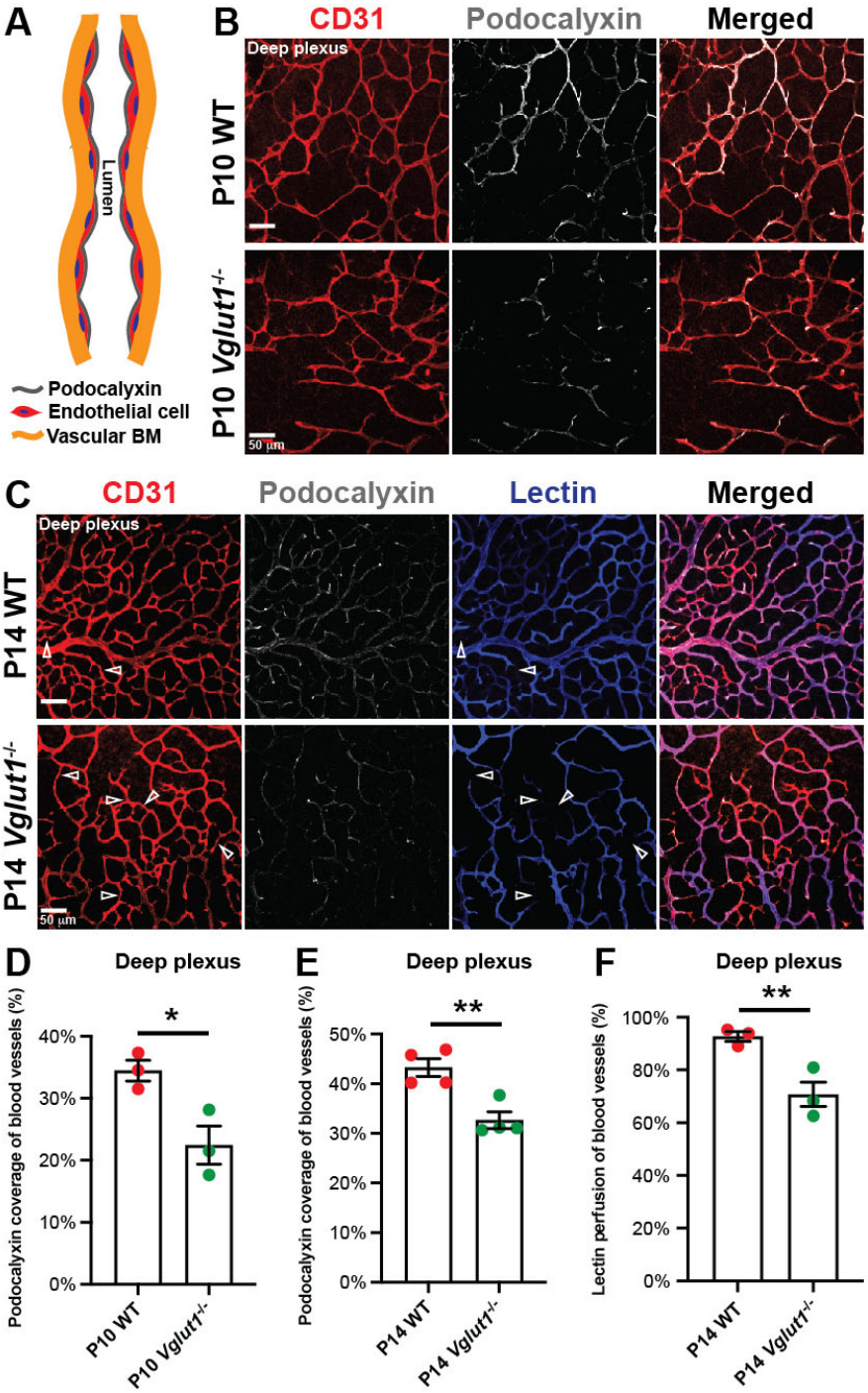

Figure 3. Deep plexus vessels in the *Vglut1*$^{-/-}$ retina are poorly perfused. A) Schematic of Podocalyxin localization on the luminal surface of ECs. BM: basement membrane. **B)** Representative images of the deep plexus of P10 WT and *Vglut1*$^{-/-}$ retinal flat mounts labeled with CD31 (red) and Podocalyxin (grey). **C)** Representative images of the deep plexus of P14 WT and *Vglut1*$^{-/-}$ retinal flat mounts labeled with CD31

.040 (red) and Podocalyxin (grey) 5 minutes after intracardiac injection of Lectin (blue). Empty arrowheads

.041 show $CD31^{+}$ vessels that are not perfused with Lectin. **D, E)** Dotted bar graphs of Podocalyxin coverage of

.042 the deep plexus in P10 (**D**) and P14 (**E**) WT and *Vglut1*$^{-/-}$ retinas (n = 3-4 mice/genotype). **F)** Dotted bar

.043 graphs of Lectin perfusion of the deep plexus in P14 WT and *Vglut1*$^{-/-}$ retinas (n=3 mice/genotype). Scale

.044 bars = 50 μm. Students t-test: *<0.05, **<0.02, NS = not significant. Error bars: Mean ± S.E.M.

.045

.046

.047

.048

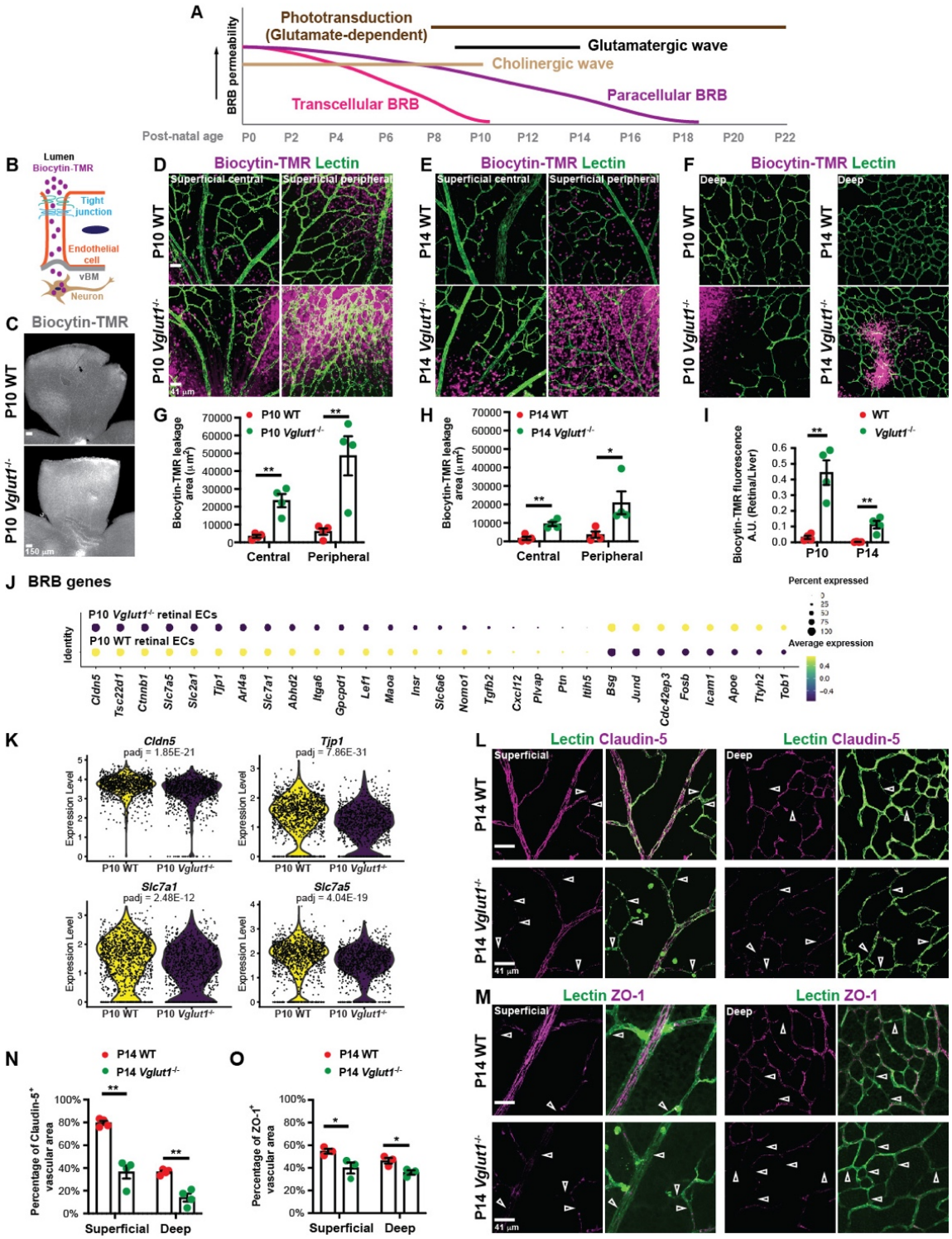

Figure 4. Paracellular BRB maturation is impaired in *Vglut1*$^{-/-}$ retina. A) Timeline of the paracellular and transcellular BRB maturation in the postnatal WT retina (P1-P22). **B)** Schematic of biocytin-TMR

.053 paracellular leakage through impaired tight junctions at the BRB; the leaked biocytin-TMR is taken up by
.054 neurons. vBM = vascular basement membrane. **C)** Representative low magnification images of P10 WT
.055 and *Vglut1*$^{-/-}$ retinal flat mounts 40 minutes after intravenous injection of biocytin-TMR, followed by PBS
.056 perfusion. **D-F)** Representative high magnification images of the superficial **(D, E)** and deep **(F)** plexuses
.057 of P10 and P14 WT and *Vglut1*$^{-/-}$ retinal flat mounts labeled with Lectin (green) 40 minutes after intravenous
.058 injection of biocytin-TMR, followed by PBS perfusion. **G-I)** Measurements of the area (**G, H**) and
.059 fluorescence intensity (**I**) of leaked biocytin-TMR in P10 and P14 WT and *Vglut1*$^{-/-}$ retinal flat mounts (n =
.060 4). BRB formation is impaired in *Vglut1*$^{-/-}$ retina. **J)** Dot plot of expression levels for BRB genes in P10 WT
.061 and *Vglut1*$^{-/-}$ retinal ECs. The dot size indicates the percent of the population expressing each marker; the
.062 color scale indicates the average level of gene expression. **K)** Violin plots of representative BRB genes in
.063 P10 WT and *Vglut1*$^{-/-}$ retinal ECs. **L)** Representative images of the superficial and deep plexuses of P14
.064 WT and *Vglut1*$^{-/-}$ retinal flat mounts stained for Claudin-5 (Cldn5; purple) and Lectin (green). Empty
.065 arrowheads point to Lectin^{+} blood vessels devoid of Claudin-5 at tight junctions. **M)** Representative images
.066 of the superficial and deep plexuses in P14 WT and *Vglut1*$^{-/-}$ retinal flat-mounts stained for ZO-1 (*Tjp1*,
.067 purple) and Lectin (green). Empty arrowheads point at Lectin^{+} blood vessels devoid of ZO-1 localization
.068 to tight junctions. **N, O)** Measurement of Claudin-5 (**N**) and ZO-1 (**O**) coverage of blood vessels in P14
.069 WT and *Vglut1*$^{-/-}$ retinas (n=4 mice / genotype). Scale bars: C = 150 μm; D, L, M = 41 μm. Students t-test:
.070 *<0.05, **<0.02. Error bars: Mean ± S.E.M.
.071

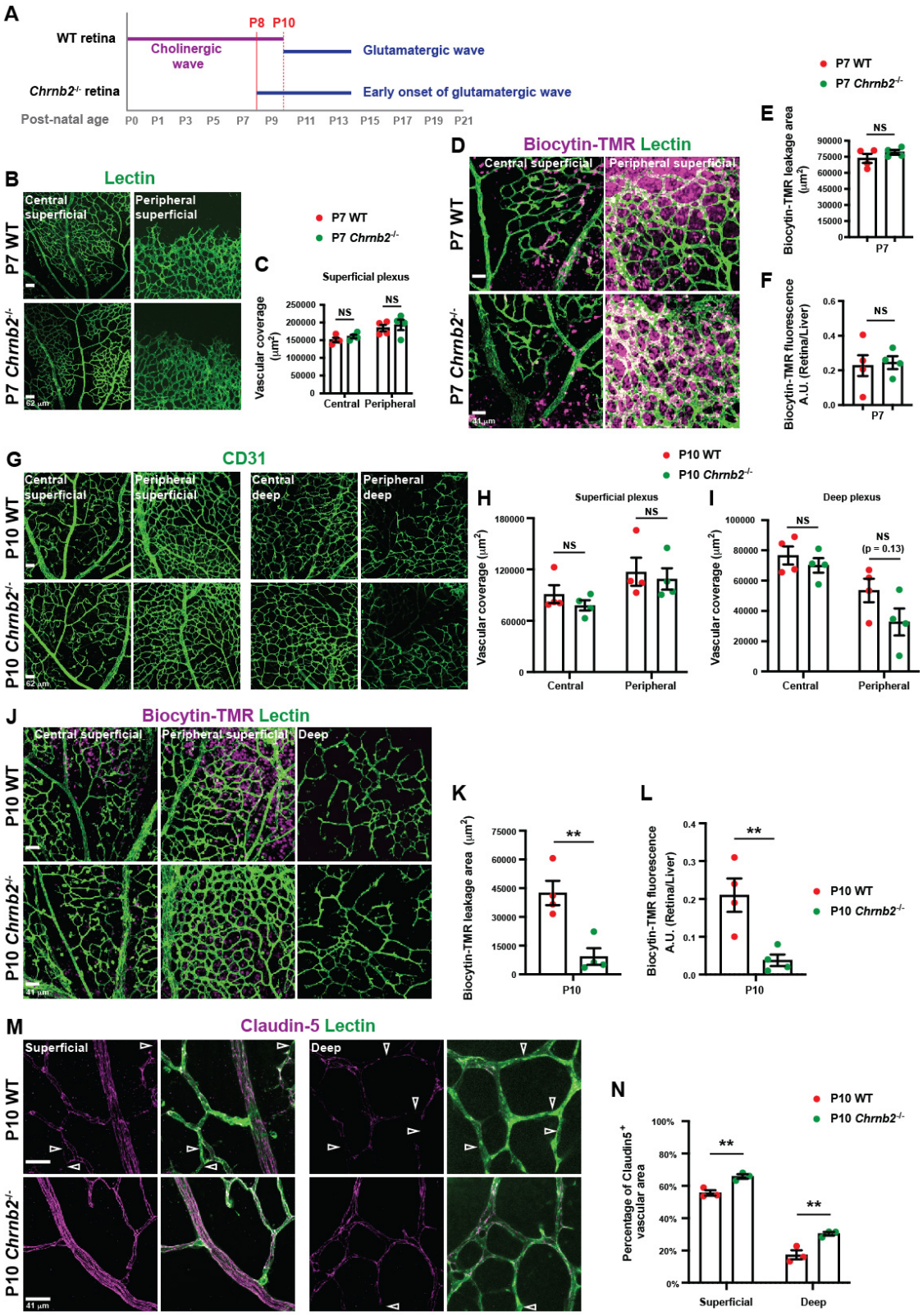

Figure 5. Paracellular BRB matures precociously in the *Chrnb2*$^{-/-}$ retina. A) Schematic diagram illustrating that glutamatergic wave begins earlier (P8) than usual (P10) in the *Chrnb2*$^{-/-}$ retina where

.076 cholinergic wave is abolished. **B)** Representative images of the superficial plexus of P7 WT and *Chrnb2*$^{-/-}$

.077 retinal flat-mounts labeled with Lectin (green). **C)** Quantification of vascular coverage in the superficial

.078 plexus of P7 WT and *Chrnb2*$^{-/-}$ retinas. **D)** Representative images of superficial and deep plexuses of P7

.079 WT and *Chrnb2*$^{-/-}$ retinal flat-mounts labeled with Lectin (green) 40 minutes after intravenous biocytin-

.080 TMR injection, followed by PBS perfusion. **E, F)** Measurements of the area (**E**) and fluorescence intensity

.081 (**F**) of leaked biocytin-TMR in P7 WT and *Chrnb2*$^{-/-}$ retinal flat-mounts (n = 4 mice / genotype). **G)**

.082 Representative images of superficial and deep plexuses of P10 WT and *Chrnb2*$^{-/-}$ retinal flat-mounts labeled

.083 with CD31 (green). **H, I)** Quantification of vascular coverage in the superficial (**H**) and deep (**I**) plexuses

.084 of P10 WT and *Chrnb2*$^{-/-}$ retinas. **J)** Representative images of superficial and deep plexuses of P10 WT and

.085 *Chrnb2*$^{-/-}$ retinal flat-mounts labeled with Lectin (green) 40 minutes after intravenous biocytin-TMR

.086 injection, followed by PBS perfusion. **K, L)** Measurements of the area (**K**) and fluorescence intensity (**L**)

.087 of leaked biocytin-TMR in P10 WT and *Chrnb2*$^{-/-}$ retinal flat-mounts (n = 4 mice / genotype). **M)**

.088 Representative images of the superficial and deep plexuses of P10 WT and *Chrnb2*$^{-/-}$ retinal flat-mounts

.089 stained for Claudin-5 (purple) and Lectin (green). Empty arrowheads point at Lectin^{+} blood vessels devoid

.090 of Claudin-5 localization to tight junctions. **N)** Measurement of Claudin-5 coverage of blood vessels in P10

.091 WT and *Chrnb2*$^{-/-}$ retinas (n = 3 mice / genotype). Scale bars: B, G = 62 μm, D, J, M = 41 μm. Students t-

.092 test: **<0.02. Error bars: Mean ± S.E.M.

.093

.094

.095

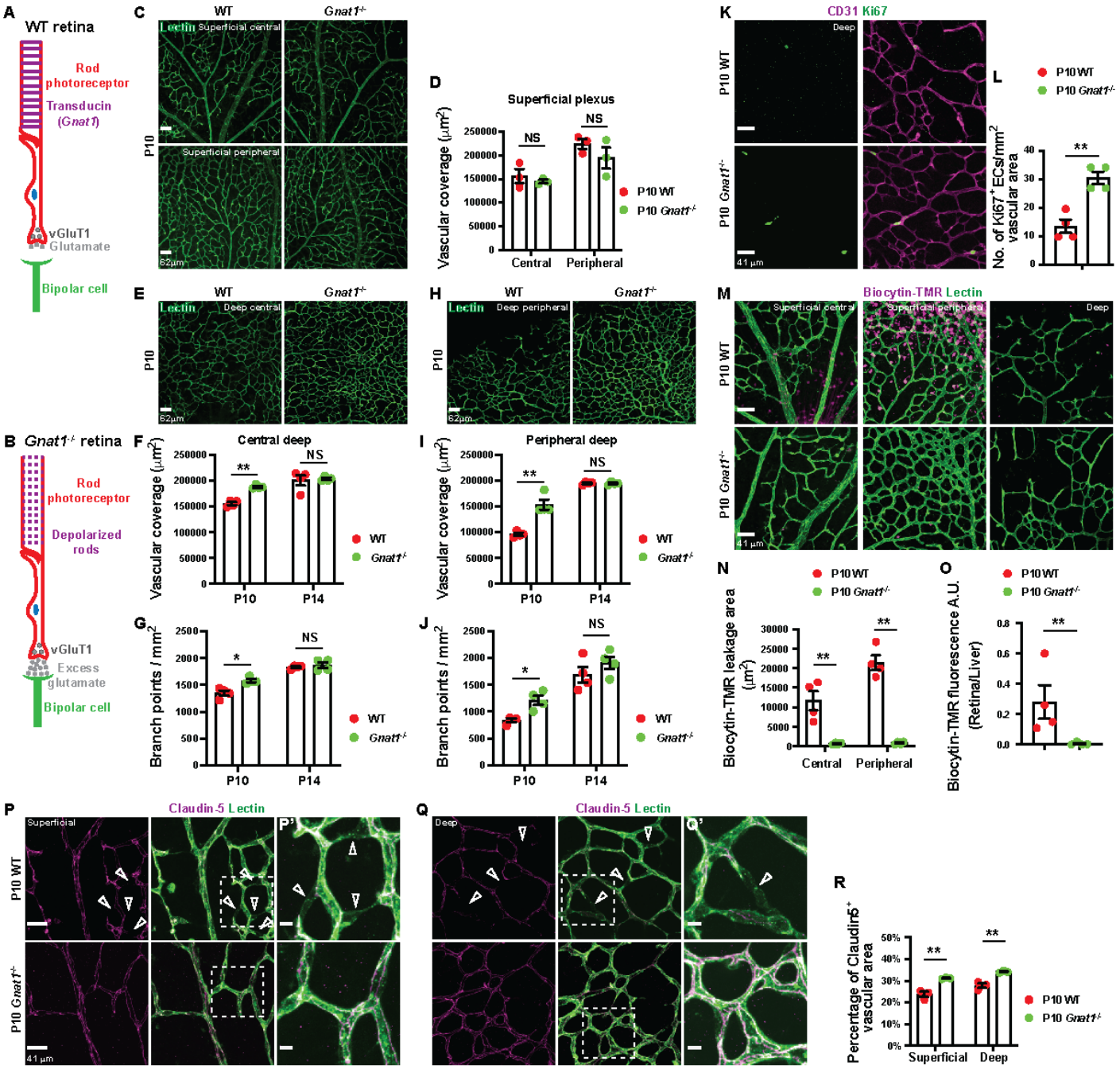

Figure 6. Deep plexus angiogenesis and paracellular BRB maturation are accelerated in the *Gnat1*$^{-/-}$ retina. A, B) Schematic diagrams of glutamate release from rod photoreceptors in WT (**A**) and *Gnat1*$^{-/-}$ (**B**) retinas. *Gnat1*$^{-/-}$ rod photoreceptors (depolarized) release excess glutamate into the synaptic cleft. **C)** Representative images of the superficial plexus in P10 WT and *Gnat1*$^{-/-}$ retinal flat-mounts stained for Lectin (green). **D)** Measurements of vascular coverage of the superficial plexus in P10 WT and *Vglut1*$^{-/-}$

103 central and peripheral retina (n = 3 mice / genotype). **E, H)** Representative images of the deep plexus in
104 P10 WT and *Gnat1*$^{-/-}$ retinal flat-mounts stained for Lectin (green). **F, G, I, J)** Measurements of vascular
105 coverage (**F, I**) and branch point density (**G, J**) of the deep plexus in P10 and P14 WT and *Gnat1*$^{-/-}$ central
106 (**F, G**) and peripheral (**I, J**) retina (n = 4 mice / genotype). **K)** Representative images of the deep plexus in
107 P10 WT and *Gnat1*$^{-/-}$ retinal flat-mounts stained for Ki67 (purple) and CD31 (green). **L)** Measurements of
108 Ki67^{+} ECs in P10 WT and *Gnat1*$^{-/-}$ retinal deep plexus (n = 4 mice / genotype). **M)** Representative images
109 of superficial and deep plexuses of P10 WT and *Gnat1*$^{-/-}$ retinal flat-mounts labeled with Lectin (green) 40
110 minutes after intravenous injection of biocytin-TMR (purple), followed by PBS perfusion. **N, O)**
111 Measurements of the area (**N**) and fluorescence intensity (**O**) of leaked biocytin-TMR in P10 WT and *Gnat1*$^{-}$
112 $^{/-}$ retinal flat-mounts (n = 4 mice / genotype). **P, Q)** Representative images of the superficial (**P**) and deep
113 (**Q**) plexuses in P10 WT and *Gnat1*$^{-/-}$ retinal flat-mounts stained for Claudin-5 (purple) and Lectin (green).
114 P' and Q' are magnified images of the corresponding boxed areas. Empty arrowheads point at Lectin^{+} blood
115 vessels devoid of Claudin-5 localization to tight junctions. **R)** Measurement of Claudin-5 coverage of blood
116 vessels in P10 WT and *Gnat1*$^{-/-}$ retinas (n = 4 mice / genotype). Scale bars: **C, E, H** = 62 μm and **K, M, P,**
117 **Q** = 41 μm. Students t-test: *<0.05, **<0.02, NS = not significant. Error bars: Mean ± S.E.M.
118

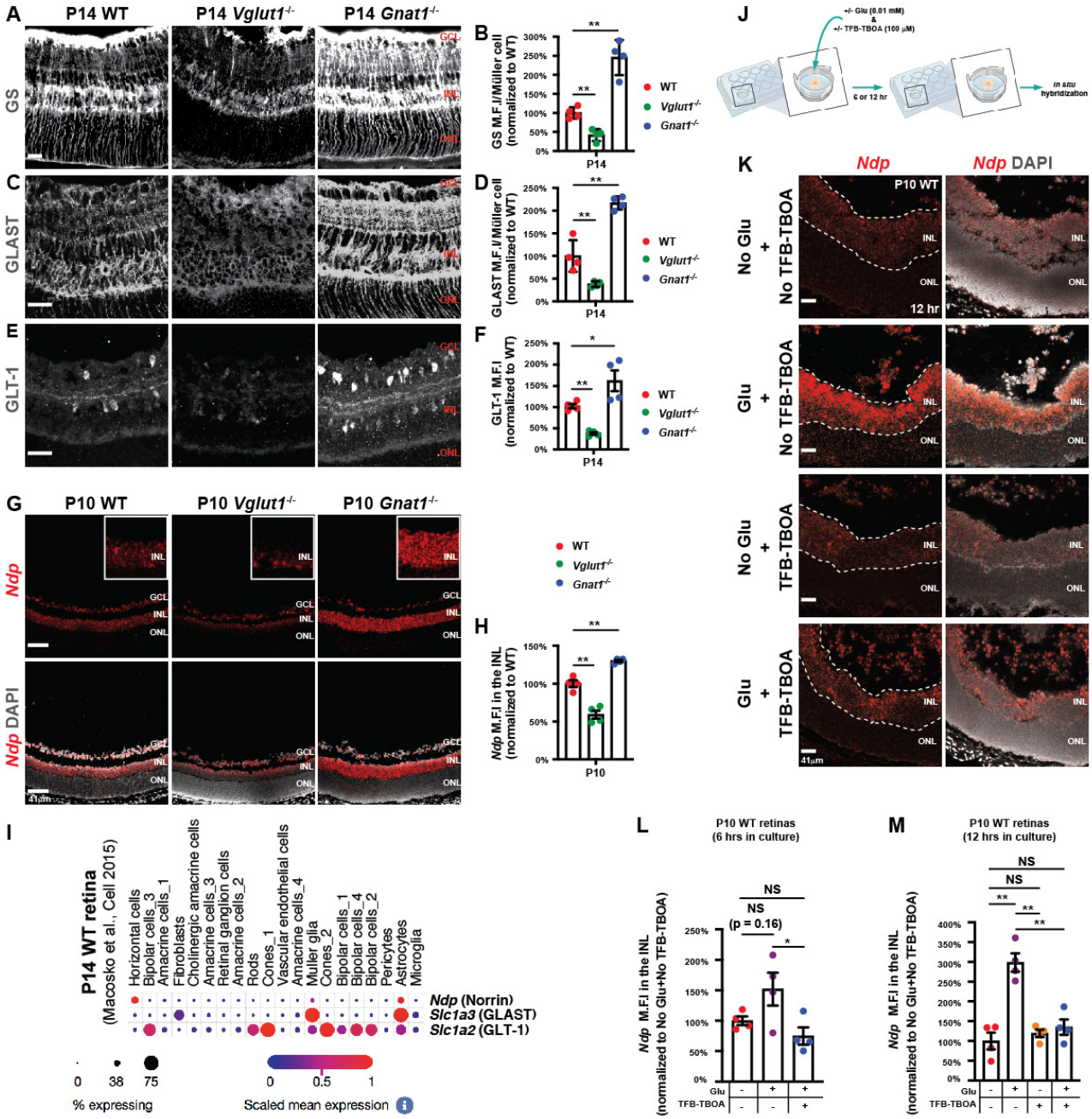

Figure 7. Expression of glutamine synthetase, glutamate transporters and Norrin are downregulated in *Vglut1*$^{-/-}$ retinas and upregulated in *Gnat1*$^{-/-}$ retinas. A, B) P14 WT, *Vglut1*$^{-/-}$ and *Gnat1*$^{-/-}$ retinal sections were stained for glutamine synthetase (GS) (**A**), and the mean fluorescence intensity (M.F.I) in the INL was quantified (**B**) for each genotype (n = 4 mice / genotype). **C, D)** P14 WT, *Vglut1*$^{-/-}$ and *Gnat1*$^{-/-}$ retinal sections were stained for GLAST (**C**), and the M.F.I in the INL was quantified (**D**) for each genotype (n = 4 mice / genotype). **E, F)** P14 WT, *Vglut1*$^{-/-}$ and *Gnat1*$^{-/-}$ retinal sections were stained for GLT-1 (**E**),

127 and the M.F.I in the INL was quantified (**F**) for each genotype (n=4 mice / genotype). **G)** Fluorescent *in*
128 *situ* hybridization of P10 WT, *Vglut1*$^{-/-}$ and *Gnat1*$^{-/-}$ retinal sections with an antisense probe against *Ndp*
129 (Norrin), followed by staining with DAPI. Norrin is expressed throughout the INL. **H)** Quantification of
130 the M.F.I of *Ndp* in the INL of P10 WT, *Vglut1*$^{-/-}$ and *Gnat1*$^{-/-}$ retinal sections (n = 4 mice / genotype). **I)**
131 Expression profiles of *Ndp*, *Slc1a3* (GLAST) and *Slc1a2* (GLT-1) in the P14 WT retina from an existing
132 scRNA-seq database [48]. *Ndp* mRNA is expressed predominantly by the horizontal cells and Müller glia in
133 the INL (small subsets of amacrine and bipolar cells also express *Ndp*). In the INL, *Slc1a3* is primarily
134 expressed by Müller glia and astrocytes, whereas *Slc1a2* is expressed in retinal neurons as well as Müller
135 glia. **J)** Schematic of *ex vivo* organotypic culture experiments. **K)** Fluorescent *in situ* hybridization of P10
136 WT retinal sections, cultured *ex vivo* for 12 hours with or without glutamate or TFB-TBOA in the media,
137 with an antisense probe against *Ndp* (*Norrin*) mRNA, followed by staining with DAPI. *Norrin* mRNA is
138 expressed throughout the INL. **L, M)** Quantification of the M.F.I of *Ndp* mRNA in the INL of P10 WT
139 retinal sections, cultured *ex vivo* for either 6 **(L)** or 12 **(M)** hours with or without glutamate or TFB-TBOA
140 in the media (n = 4 retinas / group). GCL: ganglion cell layer, INL: inner nuclear layer, ONL: outer nuclear
141 layer. Scale bars = 41 μm. One-way ANOVA: *<0.05, **<0.02, NS = not significant. Error bars: Mean ±
142 S.E.M.
143

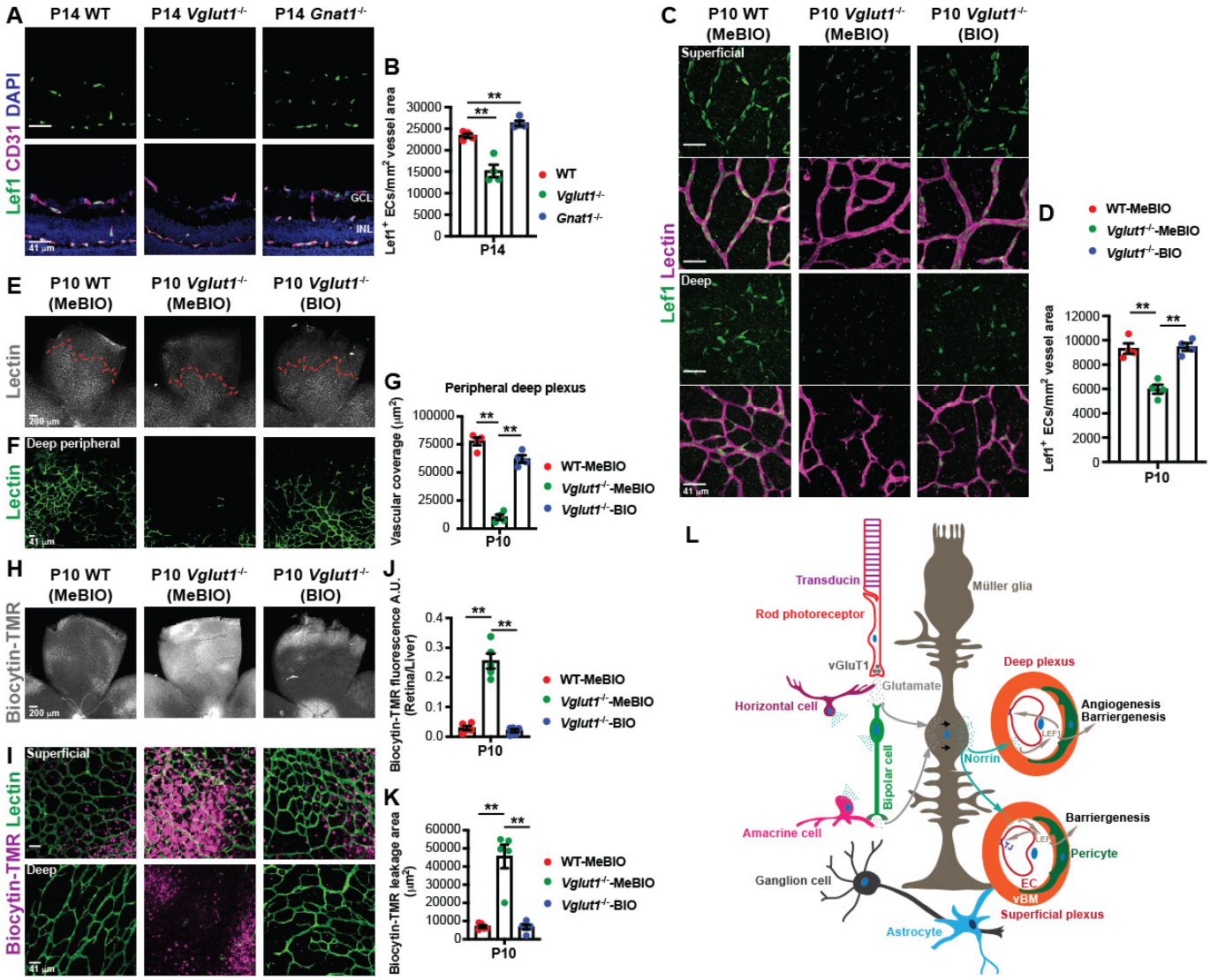

Figure 8. Upregulation of Norrin/β-catenin signaling rescues vascular deficits of the *Vglut1*$^{-/-}$ retina. **A, B)** P14 WT, *Vglut1*$^{-/-}$ and *Gnat1*$^{-/-}$ retinal sections were stained (**A**) for Lef1 (green), CD31 (purple) and DAPI (blue), and the number of Lef1^{+} ECs was quantified (**B**) for each genotype (n = 4 mice / genotype). **C, D)** MeBIO (control)- or BIO (activates Norrin/β-catenin signaling)-treated P10 WT and *Vglut1*$^{-/-}$ retinal flat-mounts were stained (**C**) with Lectin (purple) and Lef1 (green), and the number of Lef1^{+} ECs / vessel area (mm^{2}) for each treatment was quantified (**D**) for each treatment (n = 4 mice / group). BIO activates Norrin/β-catenin signaling in ECs of *Vglut1*$^{-/-}$ retinas. **E-G)** MeBIO- or BIO-treated P10 WT and *Vglut1*$^{-/-}$ retinas were stained with Lectin [low (grey; **E**) and high (green; **F**) magnifications], and vascular coverage

154 of the peripheral deep plexus was quantified (**G**) for each treatment (n = 4 mice / group). Red dotted lines
155 depict the extent of deep plexus growth. **H, I)** Representative images of flat-mount MeBIO- or BIO-treated
156 P10 WT and *Vglut1*$^{-/-}$ retinas 40 minutes after intravenous injection of biocytin-TMR [low (grey; **H**) and
157 high (purple; **I**) magnifications] and stained with Lectin (green). P10 *Vglut1*$^{-/-}$ retinas treated with MeBIO
158 have high biocytin-TMR leakage. P10 *Vglut1*$^{-/-}$ retinas treated with BIO have low biocytin-TMR leakage
159 similar to P10 WT retinas. **J, K**) Dotted bar graphs show quantification of biocytin-TMR fluorescence
160 intensity (**J**) and leakage area (**K**) (n = 5 mice / group). **L)** According to our working model, glutamate is
161 taken up into synaptic vesicles by vGluT1 (*Vglut1*), and is released into the synaptic cleft by neurons, either
162 during spontaneous glutamatergic waves (from bipolar cells) or light-dependent glutamatergic synaptic
163 activities of photoreceptors in the retina. The inhibition of glutamate release from rods after light exposure
164 is regulated by Transducin (*Gnat1*). The released glutamate signals to Müller glia and inner nuclear layer
165 (INL) neurons including horizontal, amacrine and bipolar cells. As a result, Müller glia and INL neurons
166 upregulate Norrin (*Ndp*) expression and likely its secretion; however, the relative contribution from Müller
167 glia and INL neurons on Norrin levels in this process is unclear. Glutamate-dependent secretion of Norrin
168 activates endothelial Norrin/β-catenin signaling, which in turn promotes deep plexus angiogenesis and the
169 paracellular BRB maturation in both the superficial and deep plexuses of the retina. GCL: ganglion cell
170 layer, INL: inner nuclear layer. Scale bars **A, D, G** = 41 μm, **C, F** = 200 μm. One-way ANOVA: **<0.02.
171 Error bars: Mean ± S.E.M.